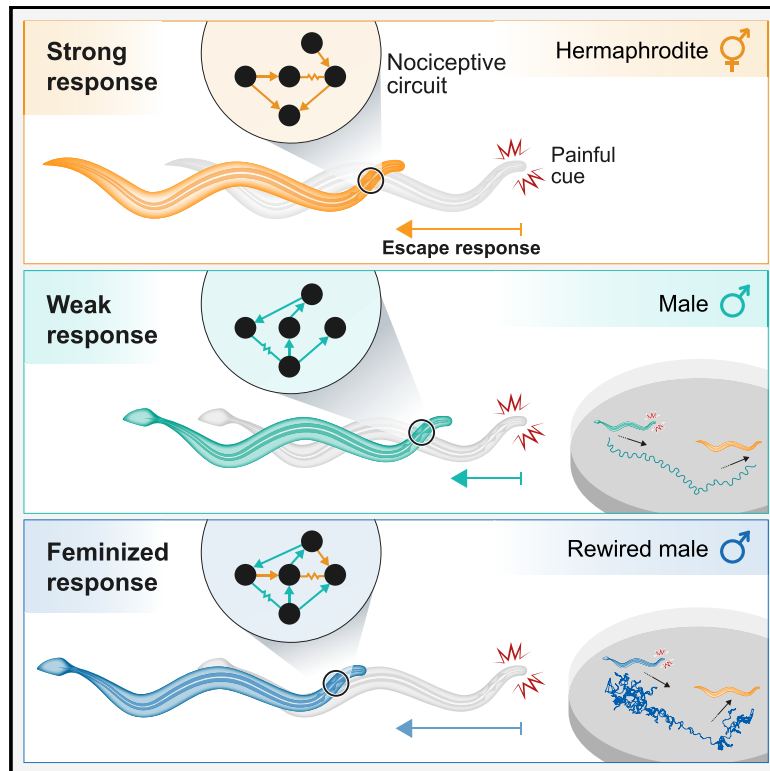**Article**

Reprogramming the topology of the nociceptive circuit in *C. elegans* reshapes sexual behavior

Graphical abstract

Authors

Vladyslava Pechuk, Gal Goldman, Yehuda Salzberg, ..., Denise M. Ferkey, Elad Schneidman, Meital Oren-Suissa

Correspondence

elad.schneidman@weizmann.ac.il (E.S.), meital.oren@weizmann.ac.il (M.O.-S.)

In brief

Pechuk et al. study the circuit for nociceptive sensing and processing in hermaphrodite and male *C. elegans*. Combining circuit models and experimental characterization, they demonstrate that network topology shapes sexually dimorphic behavior. They show that simple rewiring reprograms behavior and demonstrates its sexual implications.

Highlights

- *C. elegans* exhibits sexually dimorphic responses to nociceptive stimuli

- Computational models show that circuit topology accounts for the dimorphic behavior

- Model-based rewiring of single neurons or synapses flips sex-specific behavior

- Rewired males are compromised in finding mates when presented with aversive cues

CellPress

Article

Reprogramming the topology of the nociceptive circuit in *C. elegans* reshapes sexual behavior

Vladyslava Pechuk,[1,5] Gal Goldman,[1,5] Yehuda Salzberg,[1,5] Aditi H. Chaubey,[2] R. Aaron Bola,[2] Jonathon R. Hoffman,[2] Morgan L. Endreson,[2] Renee M. Miller,[4] Noah J. Reger,[3] Douglas S. Portman,[3] Denise M. Ferkey,[2] Elad Schneidman,[1,*] and Meital Oren-Suissa[1,6,7,*]
[1]Department of Brain Sciences, Weizmann Institute of Science, Rehovot 7610001, Israel
[2]Department of Biological Sciences, University at Buffalo, The State University of New York, Buffalo, NY 14260, USA
[3]Department of Biomedical Genetics, University of Rochester, Rochester, NY 14642, USA
[4]Department of Brain and Cognitive Sciences, University of Rochester, Rochester, NY 14627, USA
[5]These authors contributed equally
[6]Twitter: @MeitalOren
[7]Lead contact
*Correspondence: elad.schneidman@weizmann.ac.il (E.S.), meital.oren@weizmann.ac.il (M.O.-S.)
https://doi.org/10.1016/j.cub.2022.08.038

SUMMARY

The effect of the detailed connectivity of a neural circuit on its function and the resulting behavior of the organism is a key question in many neural systems. Here, we study the circuit for nociception in *C. elegans*, which is composed of the same neurons in the two sexes that are wired differently. We show that the nociceptive sensory neurons respond similarly in the two sexes, yet the animals display sexually dimorphic behaviors to the same aversive stimuli. To uncover the role of the downstream network topology in shaping behavior, we learn and simulate network models that replicate the observed dimorphic behaviors and use them to predict simple network rewirings that would switch behavior between the sexes. We then show experimentally that these subtle synaptic rewirings indeed flip behavior. Interestingly, when presented with aversive cues, rewired males were compromised in finding mating partners, suggesting that network topologies that enable efficient avoidance of noxious cues have a reproductive "cost." Our results present a deconstruction of the design of a neural circuit that controls sexual behavior and how to reprogram it.

INTRODUCTION

Sexual identity is an obvious source of variation in phenotypic traits. In sexually reproducing species, for example, females and males often respond to sensory cues in sexually dimorphic ways, reflected in their foraging, courtship, mating, and aggressive behaviors.[1,2] Such behavioral differences may originate from multiple sources or their combination: (1) sex-specific neurons, such as the courtship-related male-specific P1 neuronal cluster in *Drosophila*[3] or the hermaphrodite-specific cholinergic VC and serotonergic HSN neurons in *C. elegans*.[4] (2) Differences in the response properties of sensory neurons, as in auditory tuning in frogs,[5–9] sex-specific expression levels of G protein-coupled receptors (GPCRs) in the AWA sensory neuron in *C. elegans*,[10,11] or the activation of the mouse vomeronasal organ (VNO) in response to female and male urine.[12,13] (3) Different topologies of neural circuits over the same neurons, as reported in *C. elegans*[14] and in the pre-optic area of rats.[15,16] In mice, complex social behaviors are shaped by adaptive modulatory changes, although it is unclear whether these behaviors are a result of dimorphic connectivity or of dimorphic gene expression.[17–19] (4) Differences in synaptic strengths over the same topology.[20] (5) Different neuromodulatory effects on the circuit.[21]

To delineate the role of these potential sources in shaping dimorphic behaviors, we explored the universal trait of the noxious stimulus response. *C. elegans* present a unique opportunity to disentangle the design and function of neuronal circuits that generate dimorphic behaviors, as differences in synaptic connectivity maps between the sexes have been mapped,[4,14,22] the nervous system is accessible at the resolution of single identified neurons and connections, and the behavioral repertoire is well characterized.[23] Moreover, the small size of functional sub-networks allows circuit design to be explored computationally.[24–26]

Pain tolerance and dimorphic responses in females and males have been well documented,[27–31] whereas the underlying mechanisms have only recently been addressed.[32,33] In *C. elegans*, many noxious cues are sensed and transduced by a single pair of glutamatergic neurons, the ASHs[34] (Figure 1A), and their output is then processed by a small downstream circuit. We explored the relationship between sex-specific connectivity of the circuit (i.e., the network's topology) and the resulting behavioral output by manipulating the circuits *in silico* and *in vivo*.

We show that sensory transduction is similar between the two sexes and that differences in the topology of the circuit are sufficient to explain the observed behavioral differences. By simulating the dimorphic networks, we found a small range of circuit and neuronal parameters for which the behavioral output of the simulation matched the experimentally measured behavior. We then used our model to identify critical rewirings of the hermaphrodite and male circuits that would reshape behavior. We validated these predictions experimentally and showed that while
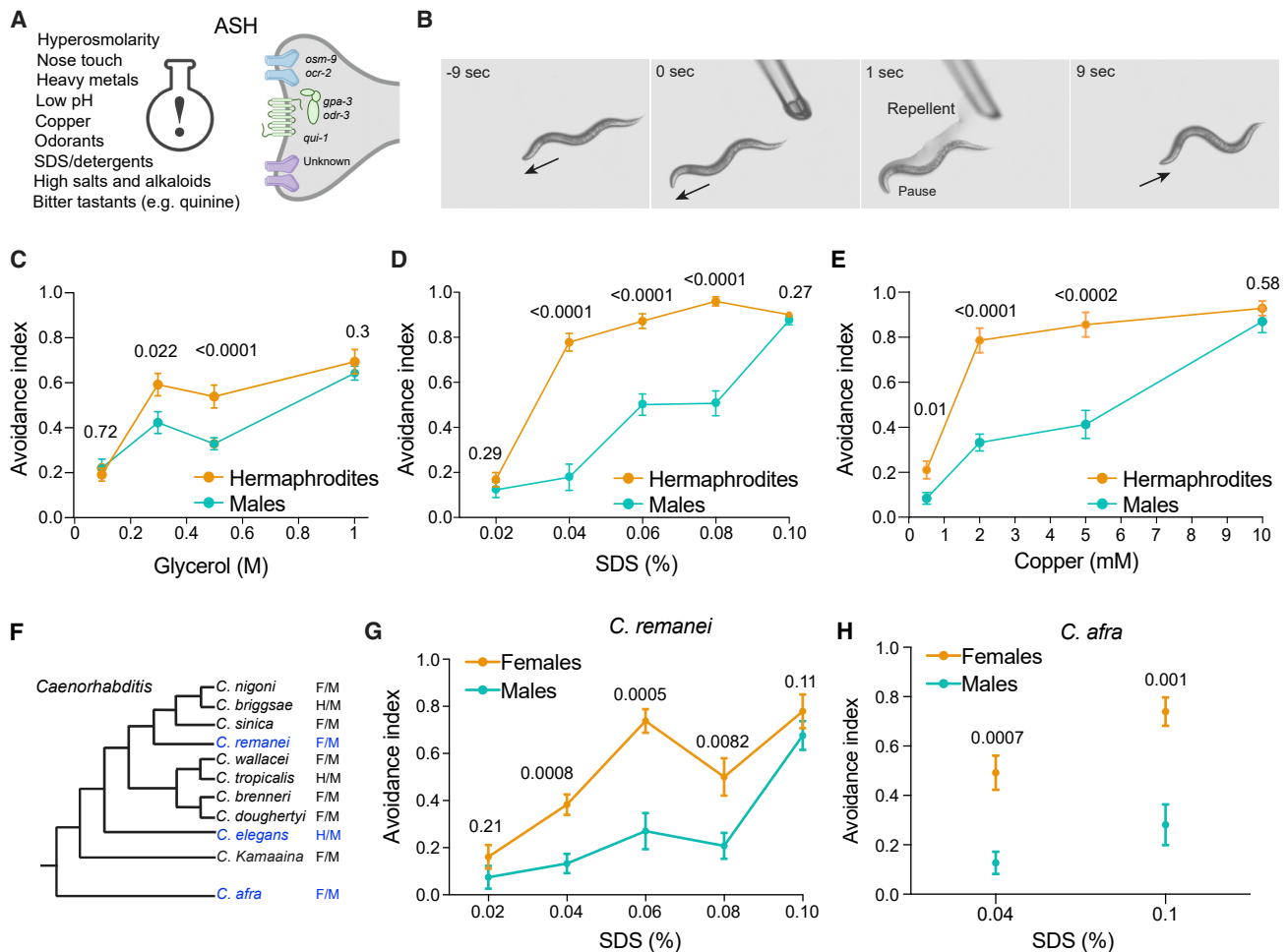
Figure 1. *C. elegans* exhibit sexually dimorphic behaviors in response to nociceptive stimuli

(A) ASH senses aversive cues through a variety of receptors and signaling molecules.

(B) Tail-drop test: as the animal moves forward (−9 s), a glass micropipette delivers a noxious cue (1 s), causing the animal to pause and initiate a reversal response (9 s). Once in contact with the tail, the drop surrounds the entire animal by capillary action.

(C–E) Dose-dependent behavioral responses to aversive stimuli: (C) glycerol, (D) SDS, and (E) copper (tail-drop assay; STAR Methods). The avoidance index represents an average of the fraction of reversal responses in 10 trials of each single animal. n = 9–15 worms per group.

(F) Phylogeny of the *Caenorhabditis* genus, where two alternative mating strategies exist.[35,36] F = female, M = male, H = hermaphrodite.

(G and H) Dimorphic behavioral responses are also present in the female-male species *C. remanei* (G) and *C. afra* (H) (tail-drop assay). n = 8–13 worms per group. Error bars are standard error of the mean (SEM). We performed a Mann-Whitney test for all comparisons. In all figures, numbers above graphs denote p values. See Figures S1 and S2.

the hermaphrodite circuit is robust to perturbations, the male circuit could be manipulated to generate the responses of the opposite sex—even by changing as little as a single connection. Moreover, males with feminized avoidance behavior were compromised in finding mates when simultaneously presented with aversive cues. Our results suggest that sexual identity sculpts neuronal circuits for the sex-specific needs of the organism, even for traits beneficial for one's survival.

RESULTS

C. elegans display sexually dimorphic behaviors in response to nociceptive stimuli

To explore the nociceptive responses of the two sexes, we presented *C. elegans* hermaphrodites and males with aversive stimuli

(Figure 1B; STAR Methods). We found that the responses of the two sexes differed for diverse types of noxious stimuli: SDS (chemical), glycerol (high osmolarity), quinine (alkaloid), and copper (heavy metal) (Figures 1C–1E, S1A–S1C, and S2A–S2D). Overall, hermaphrodites showed a stronger dose-dependent avoidance behavior compared with males. These differences were also observed in gonochoric (female-male) species of the *Caenorhabditis* genus, *C. remanei* and *C. afra* (Figures 1F–1H, S1D, S1E, and S2E), suggesting that dimorphic avoidance behavior is conserved among *Caenorhabditis*, regardless of the reproductive mode.

Similar activation of sensory neurons induces dimorphic avoidance behaviors

Having established dimorphic nociceptive behavior, we turned to explore the underlying circuits in both sexes (Figure 2A).
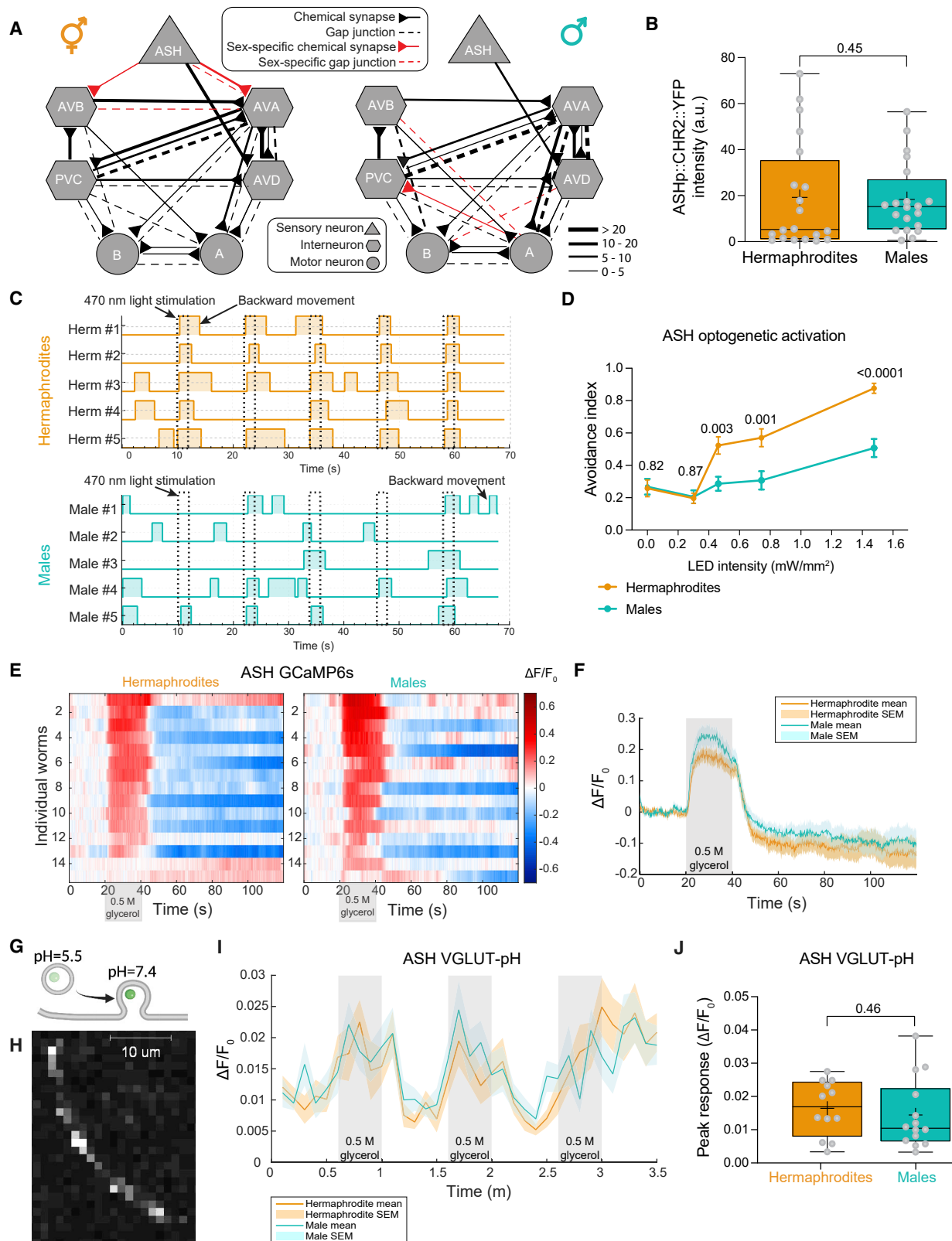
Figure 2. Sexually dimorphic behavioral choices are not encoded at the sensory level

(A) Hermaphrodite (left) versus male (right) predicted connectivity.[4,14] Chemical synapses are represented as arrows, gap junctions as dashed lines, and sex-specific connections as red arrows and dashed lines. Line width represents synaptic strength (STAR Methods).[14]

(legend continued on next page)

Downstream of the key sensory neuron ASH are the interneurons AVA and AVD, which mediate backward movement (and are excited by ASH),[37,38] and the interneurons AVB and PVC, which mediate forward movement.[39–42] The difference in activation between downstream A-type and B-type motor neurons determines the direction of movement.[40] Notably, the nociceptive circuits in hermaphrodites and males consist of the same set of neurons, which exhibit sexually dimorphic topologies.[4,14,22]

We first ascertained that the dimorphic behavior can be reproduced by optogenetically activating ASH directly using channelrhodopsin-2 (ChR2 levels do not vary between the sexes; Figure 2B). This bypasses any ASH endogenous receptors and emulates the response of ASH to arbitrary stimuli. Optogenetic activation of ASH was sufficient to elicit sexually dimorphic responses (Figure 2C). Moreover, a gradual increase in illumination intensities reproduced the dimorphic nociceptive threshold and dose-dependent response curve that was observed in the behavioral chemorepellent assays (Figures 2D and S3A).

Next, we sought to determine whether ASH displays dimorphism in its intrinsic properties. We first measured protein expression levels and subcellular localization of different receptors and signaling molecules in the two sexes. As ASH is a polymodal sensory neuron,[34,44–48] we tested the protein expression levels of several ASH receptors and signal transduction molecules (using fosmid reporters): GPA-3, OSM-10, QUI-1, OCR-2, and OSM-9. All proteins examined displayed non-dimorphic expression levels and subcellular localization, except OCR-2 levels that were slightly higher in males (Figure S3B). We then imaged the activity of ASH neurons using transgenic worms expressing GCaMP6s. For the same glycerol concentration that elicits dimorphic behavioral responses (0.5 M glycerol; Figure 1C), the calcium response of the ASH neurons was similar in the two sexes (Figures 2E, 2F, and S3C). To test whether the synaptic vesicle machinery is scaled in sex-specific manner,[49] we measured the intensity of a fosmid-based reporter for the vesicular glutamate transporter *eat-4*/VGLUT in ASH and found that it was also nondimorphic (Figures S3D–S3F). To monitor synaptic vesicle exocytosis and retrieval, we used the VGLUT-pHluorin sensor.[50] We measured glutamate secretion from ASH axons following three repeated stimulations (Figures 2G and 2H). Delivery of 0.5 M glycerol to the head to activate ASH resulted in a nondimorphic increase in VGLUT-pHluorin fluorescence (Figures 2I and 2J).

Thus, multiple lines of evidence pertaining to morphology, receptor and signal transduction, calcium response, vesicle packaging, and neurotransmitter secretion suggest that sensory transduction is non-dimorphic in this circuit.

Simulating the circuit for nociception suggests a critical role for network topology in dimorphic behavior

As sensory inputs to the circuit are nondimorphic, we turned to ask how the different connectivity patterns of the networks of hermaphrodites and males (Figure 2A) shape the dimorphic nociceptive behavior. As experimental manipulation of all possible network configurations simultaneously is impractical, we simulated the response of the two circuits to activation of the sensory neuron (Figure 2A, neuron types: ASH, AVA, AVB, AVD, PVC, A, and B). We used the difference in activations between the motor neurons (A and B) to determine the predicted direction of movement (STAR Methods).[40] As similar network activity may arise from very different sets of neuronal and network parameters,[51] and as the biophysical parameters of neurons in this circuit have not been measured simultaneously over large populations, we explored a wide range of biologically plausible values[38,52–58] (Figure 3A). For each of the seven chosen parameters, we used seven different values; overall, we simulated 7^7 = 823,543 different parameter combinations (Figures 3A and 3B).

The neurotransmitters that play a role in the modeled circuit are glutamate and acetylcholine, usually assumed to indicate excitatory connections.[59] However, cholinergic and glutamatergic inhibition has been previously demonstrated,[60,61] and expression data report both excitatory and inhibitory receptors for all the neurons in the circuit.[62] Exploring all combinations of excitation and inhibition in our circuit combined with the biophysical parameters is infeasible (2^{18} polarity options, 7^7 parameter options $\approx 10^{11}$ combinations). We therefore explored the possibility of one inhibitory connection at a time, with all biophysical parameter combinations (keeping all other 17 connections excitatory). To account for variability in connection strength between individuals, we randomly changed the synaptic strength value of each synapse by ±20% in each simulated set. For each combination of biophysical parameters, polarity, and synaptic strength, we then asked whether the activity of the simulated motor neurons will match the worms' actual behavior in response to a strong sensory stimulus ("behavioral conditions"; STAR Methods). For the hermaphrodites, we added

---

(B) Quantification and comparison of ChR2 expression levels in ASH. n = 20 per sex.

(C) Representative avoidance responses of five hermaphrodites and males to five consecutive ASH optogenetic activations (blue-light stimuli, dashed lines). Plotted boxes represent reversals.

(D) ASH activation with different LED intensities. n = 37–40 hermaphrodites, 30–40 males. See control groups without ATR in Figure S3A.

(E) Normalized and color-coded GCaMP6s calcium responses of ASH to 0.5 M glycerol. Heatmaps represent the calcium levels of individual worms. The stimulus is applied at 20–40 s.

(F) Average and SEM traces of ASH calcium responses of hermaphrodites and males. Gray background, time of stimulus delivery. See Figure S3C for a statistical comparison of peak responses.

(G) The GFP signal of the pHluorin reporter increases upon vesicular exocytosis due to change in pH.[43]

(H) Representative confocal micrograph of an ASH axon, with a visible fluorescent signal of *sra-6p::EAT-4::pHluorin*. Scale bar, 10 μm.

(I) Average and SEM traces of glutamatergic secretion from ASH axons of the two sexes, in response to three stimuli (gray background).

(J) Quantification of peak responses. Each dot is a median of three peak responses of a single worm. n = 35 hermaphrodite trials (12 animals), 38 male trials (14 animals).

(B) and (J) are box and whiskers plots, vertical line represents the median, and "+" is the mean. Same for all the following figures. We performed a Mann-Whitney test for all comparisons.
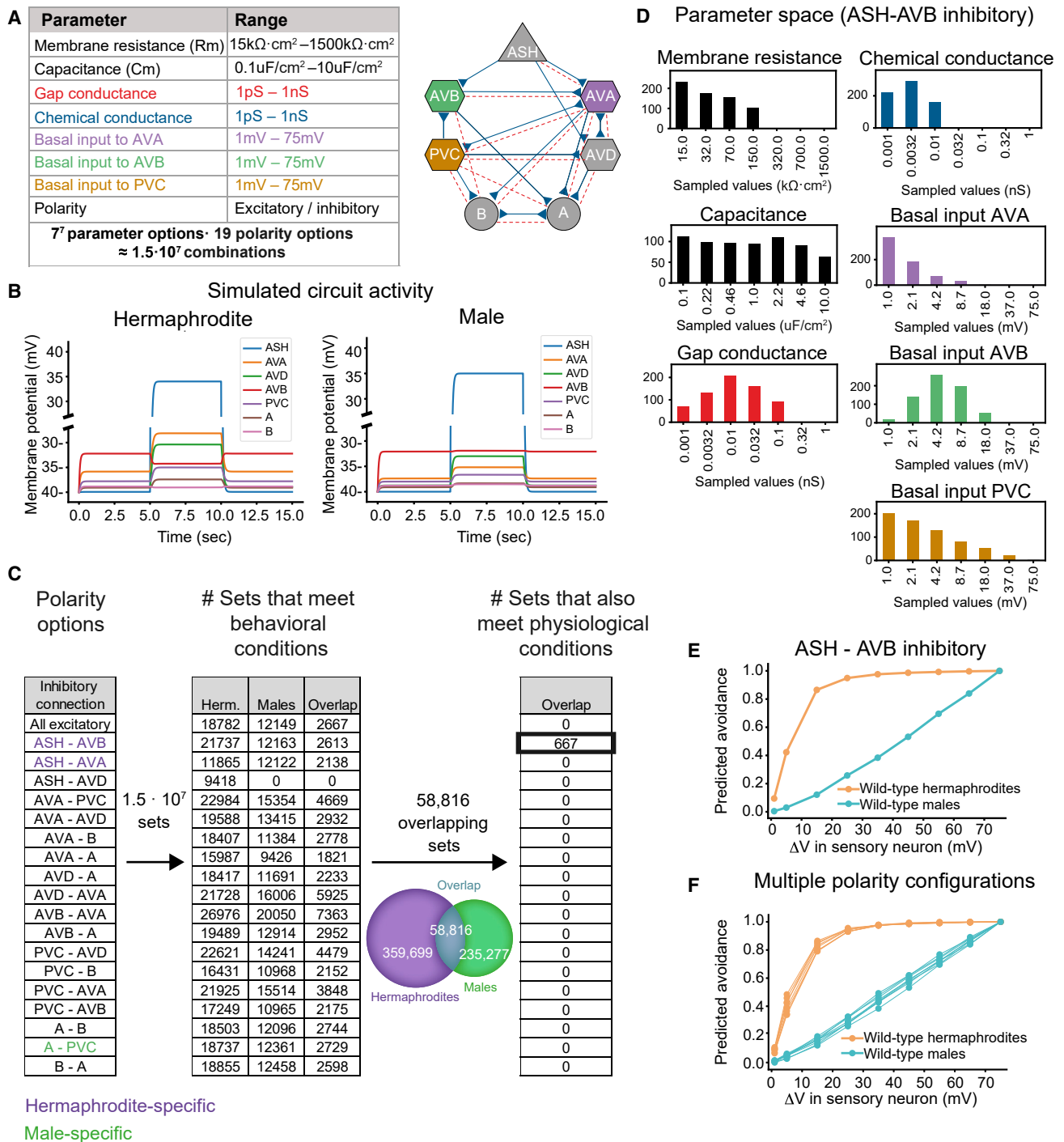
See Figure S3.

A

Parameter	Range
Membrane resistance (Rm)	15kΩ·cm² –1500kΩ·cm²
Capacitance (Cm)	0.1uF/cm² –10uF/cm²
Gap conductance	1pS – 1nS
Chemical conductance	1pS – 1nS
Basal input to AVA	1mV – 75mV
Basal input to AVB	1mV – 75mV
Basal input to PVC	1mV – 75mV
Polarity	Excitatory / inhibitory

7⁷ parameter options· 19 polarity options ≈ 1.5·10⁷ combinations

B Simulated circuit activity

Hermaphrodite / Male

C

Polarity options / # Sets that meet behavioral conditions / # Sets that also meet physiological conditions

Inhibitory connection	Herm.	Males	Overlap	Overlap
All excitatory	18782	12149	2667	0
ASH - AVB	21737	12163	2613	667
ASH - AVA	11865	12122	2138	0
ASH - AVD	9418	0	0	0
AVA - PVC	22984	15354	4669	0
AVA - AVD	19588	13415	2932	0
AVA - B	18407	11384	2778	0
AVA - A	15987	9426	1821	0
AVD - A	18417	11691	2233	0
AVD - AVA	21728	16006	5925	0
AVB - AVA	26976	20050	7363	0
AVB - A	19489	12914	2952	0
PVC - AVD	22621	14241	4479	0
PVC - B	16431	10968	2152	0
PVC - AVA	21925	15514	3848	0
PVC - AVB	17249	10965	2175	0
A - B	18503	12096	2744	0
A - PVC	18737	12361	2729	0
B - A	18855	12458	2598	0

1.5 · 10⁷ sets

58,816 overlapping sets

Overlap 58,816
359,699 Hermaphrodites / 235,277 Males

Hermaphrodite-specific
Male-specific

D Parameter space (ASH-AVB inhibitory)

Membrane resistance / Chemical conductance / Capacitance / Basal input AVA / Gap conductance / Basal input AVB / Basal input PVC

E ASH - AVB inhibitory

Predicted avoidance vs ΔV in sensory neuron (mV)
— Wild-type hermaphrodites
— Wild-type males

F Multiple polarity configurations

Predicted avoidance vs ΔV in sensory neuron (mV)
— Wild-type hermaphrodites
— Wild-type males

Figure 3. Simulation of the circuit for nociceptive behaviors recapitulates the behavioral differences between the sexes

(A) Summary of the biophysical and polarity parameters. A schematic representation of the seven neuron types used in our model is shown to the right. The different colors represent different parameter categories.

(B) Representative simulation of the membrane potential of the cells in the circuit, for the hermaphrodite (left) and the male (right). The detection of an aversive stimulus was simulated using input current to the sensory neuron ASH (5–10 s). Constant basal input was given to the interneurons, such that it increased their membrane potentials as follows: 4.2 mV AVA, 1 mV PVC, and 8.7 mV AVB (STAR Methods). Biophysical parameters used: 150 kΩ·cm² resistance, 0.46 $\frac{uF}{cm^2}$ capacitance, 1 pS chemical conductance, and 3.2 pS gap conductance. Noise was not simulated.

(C) The number of parameter sets that met two types of conditions: behavioral and physiological (STAR Methods), divided into polarity configurations. Each row represents the number of sets that met the requirements with a different chemical connection simulated as inhibitory. Physiological conditions were tested only

(legend continued on next page)

physiological requirements, based on measurements of anticorrelated activity between A and B motor neurons and between the AVA and AVB neurons[40] ("physiological conditions"; STAR Methods). The "appropriate sets" were combinations of biophysical parameters and polarity that met the behavioral conditions for both sexes and the physiological conditions for the hermaphrodites (Figure 3C). We found that while almost all polarity configurations had a set of biophysical parameters that could adhere by the behavioral conditions, the inhibitory connection between ASH-AVB was essential for meeting the physiological conditions (Figure 3C). We further explored polarity configurations that had other inhibitory connections in addition to the ASH-AVB one and found that they had a minor effect on the number of appropriate sets (Figure S4A). We therefore continued to explore the topology with inhibition only in the ASH-AVB connection (Figures 3B and 3C). We note that the range of values explored for the biophysical parameters was validated by the fact that most potential values were represented in at least one appropriate set (Figure 3D).

Importantly, the average response curves predicted by the model over the appropriate sets (which were the same for the two sexes) replicated the distinct behavior of each sex observed experimentally (Figure 3E). Again, adding inhibitory connections to that of ASH-AVB did not change the model's predictions (Figure 3F). We conclude that the differences in topology alone are sufficient to reproduce the dimorphic behavior between the sexes.

Sexually dimorphic interneuron activation in response to a nociceptive cue

We next turned to the network downstream to ASH. ASH connections to the interneurons are dimorphic (Figure 2A), and the simulated networks predict clear dimorphic activation of the interneurons (Figure 4A). We therefore used calcium imaging to measure the activity of the AVA interneurons. We found distinct sex-biased responses to 0.5 M glycerol in AVA: (1) the peak calcium levels were higher in hermaphrodites than in males (Figures 4B–4D). (2) While the calcium signals in hermaphrodites decayed at a slow pace and varied in time, those in the male AVA lasted only while the stimulus was delivered, but dropped immediately upon its withdrawal (Figures 4B, 4C, and 4E). As we found the behavioral responses of the two sexes to be similar for strong stimuli (Figure 1C), we also measured AVA activity in response to a higher glycerol concentration. Indeed, at 1 M glycerol, the activity pattern of male AVA better resembled that of the hermaphrodite (Figures 4F and 4G)—marked by a comparable peak intensity—but the response duration remained dimorphic (Figures 4H and 4I). Taken together, the predictions of our simulations and the experimental measurements of AVA suggest that sensory-to-interneuron connectivity plays a key role in the dimorphic behavior.

Rewiring of specific neurons switches behavior in a sexually dimorphic manner

We used our model to identify critical rewiring of the network's connections that would suffice to switch behavior between the sexes. We first simulated "feminization" and "masculinization" of individual neurons in the network, namely, replacing all the connections of a specific neuron in one sex with the connections of the same neuron in the other sex (STAR Methods). For ASH, both masculinization and feminization resulted in behavior that resembled that of the opposite sex (Figure 5A, middle panel), and similar results were found for manipulation of the B motor neuron (Figure S5E). Simulating AVA feminization in males resulted in a response curve that resembled the predicted wild-type hermaphrodite response, whereas simulating AVA masculinization in hermaphrodite had only a minor effect on the predicted behavior (Figure 5A, right panel). Similar results were found for AVB and AVD neuron manipulations (Figures S5A and S5B). The predicted effects of feminizing or masculinizing ASH and AVA were similar with additional polarity combinations, including the inhibitory ASH-AVB connection (Figures S4B and S4C). Thus, our model predicts that changing the connectivity of individual neurons to that of the opposite sex can be sufficient to switch the behavioral response of the worm.

We then tested these predictions experimentally and explored whether manipulating the sex-determination pathway of the worm to genetically feminize (tra-2 expression) or masculinize (fem-3 expression) specific neurons[64–66] (STAR Methods) will affect connectivity and behavior. To verify that the genetic sex reversal manipulations resulted in the desired synaptic connectivity changes, we trans-synaptically labeled the connection between ASH and AVA using in vivo biotin labeling of intracellular contact (iBLINC; Figures 5B–5D).[63] First, we analyzed GFP puncta of the ASH-AVA connection temporally in wild-type animals, confirming that the connection is hermaphrodite specific in adults (Figure S6A). Second, we quantified the synaptic connections in sex-reversed animals and found, surprisingly, that in hermaphrodites, genetic sex reversals did not result in changes to ASH-AVA connectivity. However, in males, pan-sensory feminization resulted in the formation of ectopic ASH-AVA synapses (Figure 5E).

We then tested whether the sex reversal of single neurons changed the behavior induced by optogenetic stimulation of animals expressing ASH-ChR2. We found that, indeed, pan-sensory feminization resulted in sex reversal of the male behavior (Figure 5F), in agreement with our model's prediction. Pan-sensory or AVA masculinization, however, was not sufficient to change the hermaphrodite's behavior (Figures 5F and 5G), in line with the unchanged synaptic connectivity (Figure 5E).

Our transsynaptic labeling between ASH and AVA enabled us to assess the developmental aspect of these dimorphic

for the hermaphrodites' connectivity. Purple connections are hermaphrodite specific; green connections are male specific. For the sex-specific connections, the opposite sex remained in the all-excitatory state.

(D) Distribution of the biophysical parameters' values in the sets that met all behavioral conditions for both sexes and all physiological conditions for the hermaphrodites (ASH-AVB inhibitory). x axis, seven values per parameter; y axis, number of appropriate sets.

(E) Networks using the same set of parameters for both sexes capture the behavioral differences between them. x axis, voltage increase in the sensory neuron following the stimulus (STAR Methods). y axis, predicted avoidance averaged over all appropriate sets (667 sets).

(F) The dimorphic behavior is maintained throughout different polarity configurations. We tested all of the combinations of excitation and inhibition in the following connections: ASH-AVB, AVB-AVA, A-B, and B-A (overall 16 options; see Figure S4A).
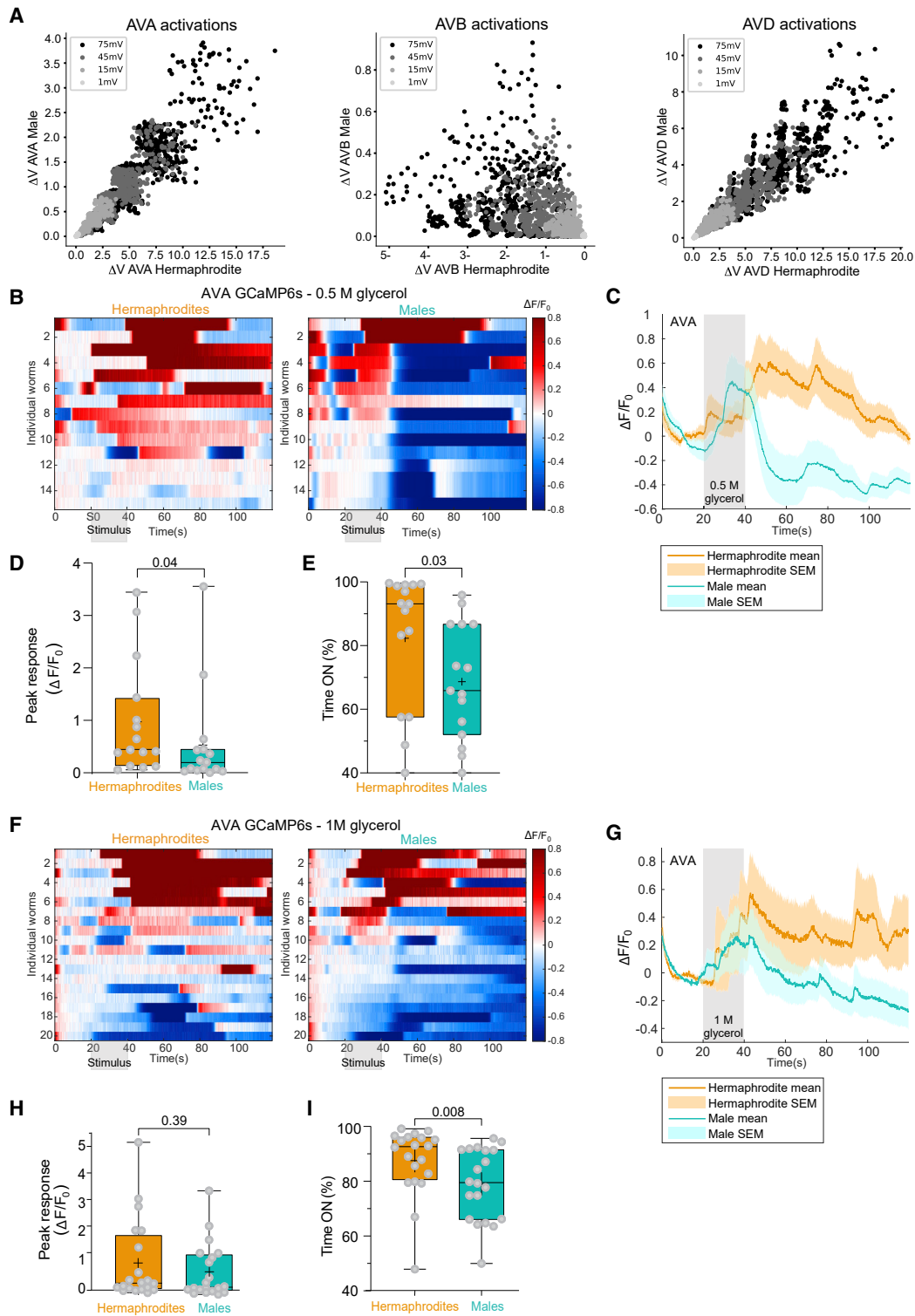
Figure 4. Sexually dimorphic interneuron responses to aversive cues

(A) The simulated change in membrane potential induced by the sensory stimulus in the interneurons directly downstream to ASH in at least one sex (AVA, AVB, AVD, left to right). x axis, change in the hermaphrodites (mV); y axis, change in the males (mV). Each point represents a different parameters' set.

(B–I) GCaMP6s calcium responses of AVA interneurons to 0.5 M (B–E, n = 15 animals per sex) and 1 M (F–I, n = 20 animals per sex) glycerol. (B and F) Heatmaps of individual animals representing the normalized calcium levels (color coded). Stimulus is applied at 20–40 s. (C and G) Average and SEM traces of AVA calcium levels. Response intensity (in C) and duration (in C and G) are sexually dimorphic. (D and H) Quantification of peak responses. (E and I) Quantification of response duration. We performed a Mann-Whitney test.
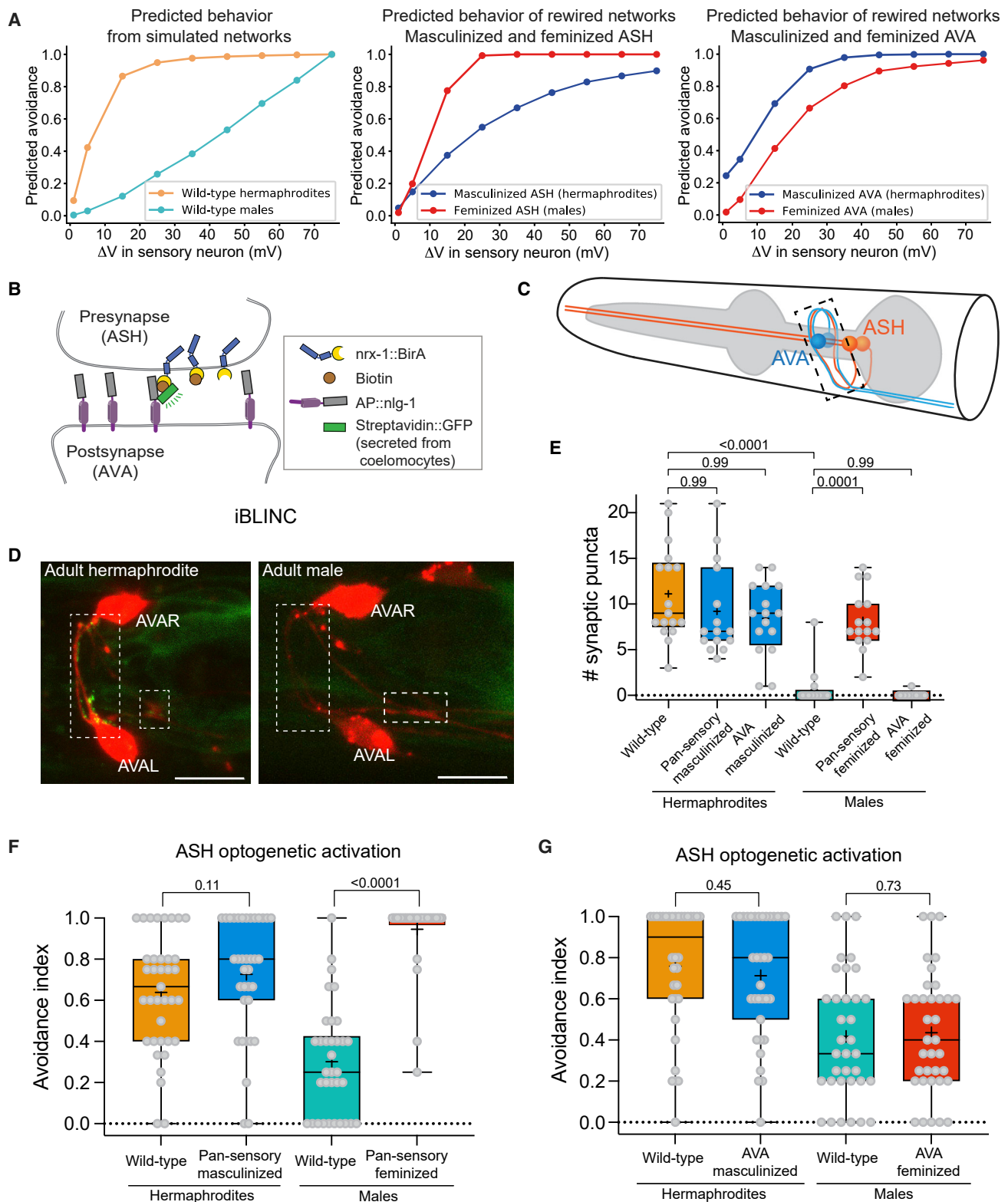
Figure 5. The sexual identity of the sensory neurons shapes the avoidance behavior in a sexually dimorphic manner

(A) Model predictions of the escape response in wild-type worms (left), worms with feminized or masculinized ASH (middle), and AVA (right). Predicted avoidance at each voltage point is calculated by averaging the movement direction results of the appropriate parameters' sets.

(B) Schematic of iBLINC.[63]

connections. Synapses are first observed at the third larval stage in both sexes, but then are sex-specifically removed in males (Figure S6A). In line with the non-dimorphic synaptic connectivity at this stage, juvenile animals (L3) respond in a nondimorphic manner to the nociceptive 0.5 M glycerol stimulus (Figure S6B), suggesting that the sexually dimorphic response to aversive stimuli is unique to the adult nervous system. Taken together, our results suggest that the hermaphrodites' connectivity map and resulting nociceptive behavior are more robust compared with those of males.

Rewiring a single synapse is sufficient to flip behavior to that of the opposite sex

Given the success of changing behavior by sex reversal at the neuronal level, we turned to ask what would be the behavioral effect of rewiring individual synapses. We used our simulated networks to explore the potential effect of flipping a single synapse, or pairs of synaptic connections simultaneously. Our simulations predict that removing a single hermaphrodite-specific connection would not induce a male-like response (Figures 6A and S7). However, it predicts that the addition of hermaphrodite-specific connections to males can induce a behavioral switch (Figures 6B and S7). These results are not affected by switching additional connections to be inhibitory (Figures S4D and S4E). Neither sex is predicted to be affected by the removal or addition of male-specific connections (Figure S7). We then manipulated the ASH-AVA connection experimentally and generated a transgenic strain carrying a mammalian connexin36-mediated synthetic gap junction[67] between both neurons (Figure 6C). To verify that the synthetic gap junction is expressed and localized properly, we imaged the fluorescent connexin36 tags. ASH-connexin36 puncta coincided with AVA-connexin36 puncta and localized along the overlapping region between the two neurons at the nerve ring, as expected (Figure 6D). We measured the behavior of these males in comparison with wild type ones and found that the specific rewiring increased the frequency of reversals, close to the values measured in wild-type hermaphrodites (Figure 6E), in agreement with the model's predictions (Figures 1C and 6B).

Rewired males are less successful in finding a mate

Our rewiring experiments enabled us to explore an even wider behavioral implication of the network's topology, and ask how rewiring might affect male behavior under more natural environmental conditions. We therefore tested single males in a compound environment containing a confined group of hermaphrodites, serving as an attractive sensory cue, while receiving repeated nociceptive stimuli, delivered optogenetically

(Figure 7A). We compared the behavior of wild-type males to that of pan-sensory feminized males (in which the ASH-AVA synaptic connection exists), both expressing ChR2 in ASH. We recall that in wild-type males ASH activation generates a significantly reduced escape response compared with hermaphrodites (Figure 2D), whereas the pan-sensory feminized ones respond in a hermaphrodite-like manner (Figure 5F). We found that activating ASH in these males significantly prolonged the time required for them to reach the hermaphrodites (Figures 7B and 7C). Pan-sensory feminized males without all-trans-retinal (ATR) showed normal attraction toward hermaphrodites, indicating that the genetic manipulation did not alter their sensory attraction to hermaphrodites. These results suggest that having a topology that enables a low nociceptive threshold and a hermaphrodite-like avoidance of noxious cues in males would incur a "cost" in terms of finding mates.

DISCUSSION

We explored the design of a neural circuit composed of sex-shared neurons that control the fundamental trait of response to pain sensation. We extensively analyzed the sensory responses to stimuli, which have been mostly neglected in studies deciphering sexually dimorphic behaviors,[5,68] and consequently focused on differences downstream to the sensory level.[69–71] We found that *C. elegans* exhibit sexually dimorphic nociceptive behaviors that do not originate from the sensory neurons but are instead mediated by the downstream circuits that are connected in a dimorphic manner.

We simulated the nociceptive circuits and identified a small number of biophysical parameter sets that replicated the behavioral results measured experimentally. Capturing the dimorphic behavior using the same biophysical parameters for both sexes showed that topology alone may be enough to explain the behavioral differences. We acknowledge, however, that our models did not consider biophysical noise in the neurons or synapses, neuropeptide signaling, asymmetry in the activity of electrical synapses, or differences in the parameters of the neurons within the same circuit. Extending the models to include these features might reveal the contributions of nontopological sources to the dimorphic behavior. Similarly, while we have focused on the nociceptive circuit itself, its member neurons are connected to neurons outside the circuit,[72] which in turn may also contribute to behavioral differences. Nonetheless, the accuracy of our simple model and the validation of its predictions experimentally suggest that we indeed identified which dimorphic connectivity structures shape behavior and how to reprogram behavior by changing connectivity.

(C) Illustration of the contact area (dashed rectangle) between ASH (left and right, orange) and AVA (left and right, blue) at the nerve ring along the ASH axon.

(D) Representative confocal micrographs of an adult hermaphrodite and male, showing iBLINC GFP puncta only in hermaphrodites at the contact areas of ASH-AVA (dashed rectangles). AVA neurons are labeled with cytoplasmic mCherry. Scale bars, 10 μm.

(E) Quantification of ASH-AVA iBLINC GFP puncta in hermaphrodites and males: wild-type and sex-reversed animals. osm-5 promoter drives expression in all ciliated neurons ("pan-sensory"). n = 15–18 animals per group.

(F) Avoidance index for ASH optogenetic activation in wild-type or pan-sensory sex-reversed animals. LED intensity is ∼1.47 mW/mm^2. n = 33–37 animals per group.

(G) ASH optogenetic activation in wild-type worms and worms with masculinized or feminized AVA. LED intensity is ∼1.47 mW/mm^2. n = 34–36 animals per group.

In (E), we performed a Kruskal-Wallis test followed by Dunn's multiple comparison test; in (F) and (G), we performed a Mann-Whitney test.
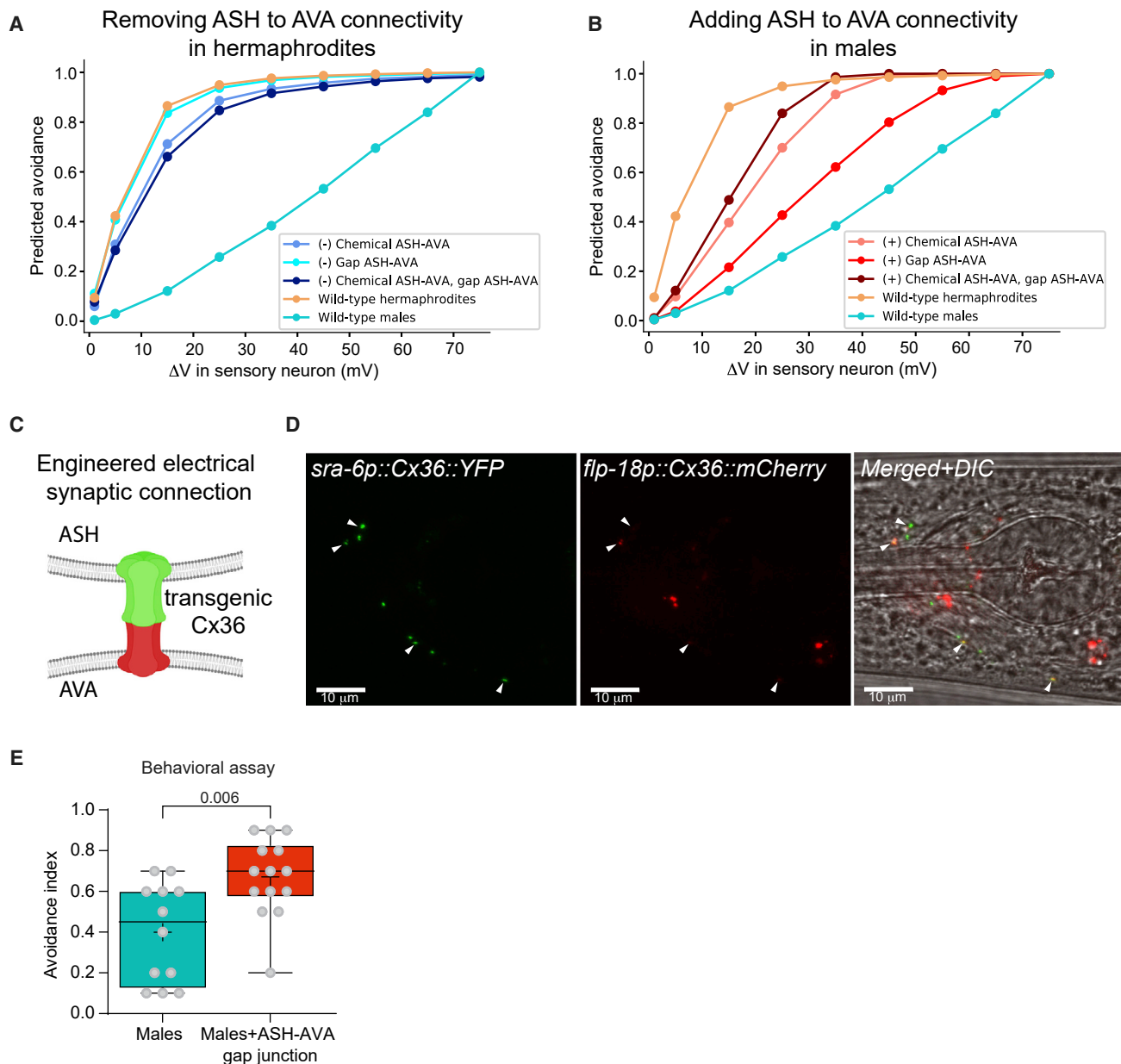
See Figures S4–S6.

A Removing ASH to AVA connectivity in hermaphrodites

B Adding ASH to AVA connectivity in males

C Engineered electrical synaptic connection

D

E Behavioral assay

Figure 6. Rewiring of a single connection in the circuit is sufficient to feminize male avoidance behavior

(A) Model predictions of the escape response in wild-type worms and hermaphrodites without the ASH-AVA connection (chemical, electrical, or both).

(B) Model predictions of the escape response in wild-type worms and males with an additional connection between ASH and AVA (chemical, electrical, or both). The predicted avoidance at each voltage point is calculated by averaging the movement results of the appropriate parameters' sets of the model.

(C) A fluorescently tagged codon-optimized mouse connexin Cx36 is expressed under the ASH (YFP) and AVA (mCherry) promoters.[67]

(D) Representative confocal micrographs of a male expressing a synthetic ASH-AVA electrical synapse. *ASHp::Cx36::YFP* and *AVAp::Cx36::mCherry* puncta (white arrowheads) colocalize along the contact area of ASH and AVA. Scale bar, 10 μm.

(E) Tail-drop assay with a 0.5 M glycerol stimulus, males with a gap junction (n = 14) between ASH and AVA compared with wild-type males (n = 12). We performed a Mann-Whitney test.

See Figures S4 and S7.

The models predicted that hermaphrodite behavior would be more robust to connectivity perturbations than the male behavior. The experimental results support this notion—sex reversal of individual neurons was not sufficient to change the synaptic connectivity and behavior of hermaphrodites, while for the males, sensory sex reversal flipped synaptic connectivity and the resulting behavior. Thus, the sexual identity of ASH dictates the connectivity in males but not in hermaphrodites. This surprising result is in contrast to previous studies that used reciprocal sex reversals to demonstrate that neuronal
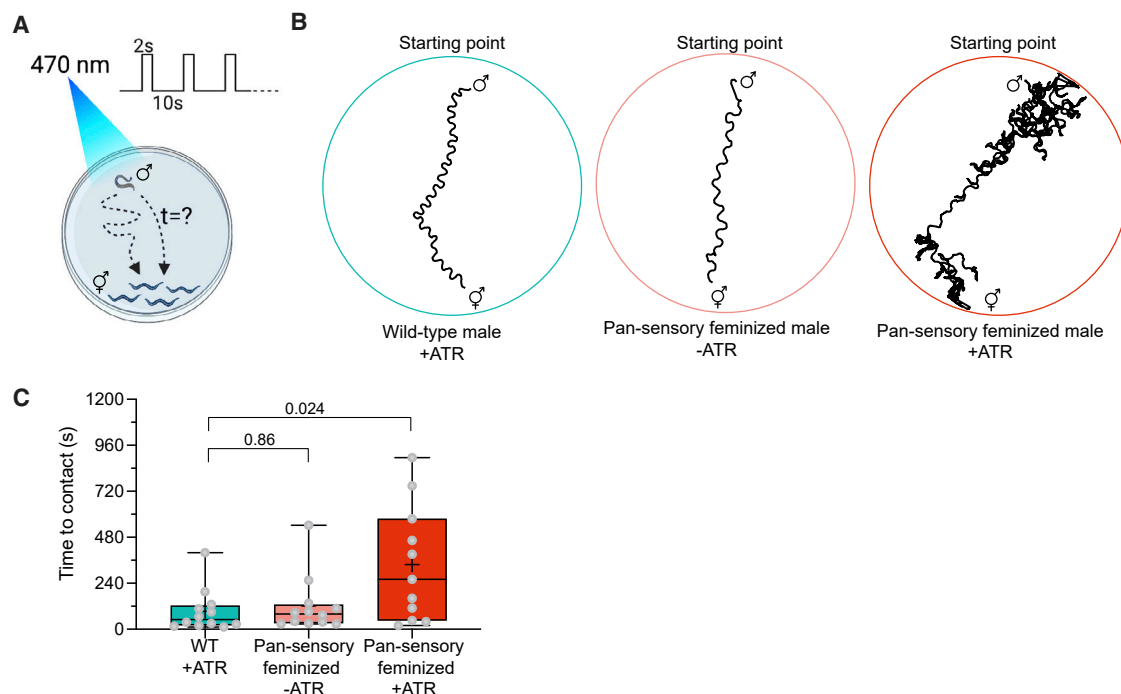
Figure 7. Feminized avoidance behavior impedes males' ability to reach a mate

(A) Repetitive optogenetic stimulations of ASH are applied while the male is searching for the immobilized hermaphrodites. The time it takes the male to contact a hermaphrodite is quantified (STAR Methods).

(B) Representative traces of a WT male +ATR (left), a pan-sensory feminized male −ATR (middle), and a pan-sensory feminized male +ATR (right).

(C) Quantification of the time to contact of WT males with ATR, pan-sensory feminized males without ATR, and pan-sensory feminized males with ATR. n = 11–12 males per group.

We performed a Kruskal-Wallis test followed by Dunn's multiple comparison test.

sexual identity functions cell autonomously.[49,65,66,73,74] Our results may point to non-autonomous effects that are mediated either by suppressive signals from the hermaphrodite body or the absence of positive signals coming from the male body. Alternatively, a cell-autonomous signal independent of the known sex-determination pathway could control hermaphrodite connectivity. Another possibility is an involvement of a third cell that instructs whether the ASH-AVA synapse should be pruned only in hermaphrodites. The presence of mechanisms that maintain the hermaphrodite robustness to changes suggests that the low nociceptive threshold in hermaphrodites is an important property.

The imaging of interneurons in response to aversive stimuli revealed variability in their activity across individuals, where some males exhibited hermaphrodite-like neuronal activity levels (Figure 4B). Such inter-individual and sex-dependent differences have been reported for different organisms,[75–79] but the underlying mechanisms generating individuality are unclear. The hermaphrodite-like activity of this neuron in some of the males may arise from variability in connectivity between individual males (e.g., a weak connection between ASH-AVA) and could also reflect developmental and evolutionary implications. The differences between adult worms reported in Witvliet et al.,[80] and in comparison with White et al.[4] and Cook et al.,[14] reflect that such variability is probably prevalent.

Sexual selection and natural selection are viewed as evolutionary forces that occasionally act in a contradictory manner

in cases where sexual selection selects for phenotypes that are not favored by natural selection.[81,82] The fact that the reprogrammed sensory-feminized males demonstrate increased sensitivity to aversive stimuli, as well as decreased efficiency in making contact with hermaphrodites in the presence of nociceptive cues, shows that there is a trade-off between these two behaviors. The Darwinian notion that most sex differences are the result of sexual selection suggests here that the natural topology of males makes them less pain sensitive and therefore more risk takers. Thus, males would suffer a reproductive "cost" for a topology that enables a more efficient avoidance of noxious cues. This is further supported by the behavioral experiments in female-male *Caenorhabditis* species, which demonstrate that the sexually dimorphic response to nociceptive cues is conserved regardless of mating strategy.

STAR★METHODS

Detailed methods are provided in the online version of this paper and include the following:

- KEY RESOURCES TABLE
- RESOURCE AVAILABILITY
    - Lead contact
    - Materials availability
    - Data and code availability
- EXPERIMENTAL MODEL AND SUBJECT DETAILS

Current Biology
Article

CellPress
OPEN ACCESS

- **METHOD DETAILS**
  - Repellent assay – tail-drop
  - Repellent assay – head-drop
  - Microfluidic chip fabrication and calcium imaging
  - pHluorin imaging
  - Optogenetics
  - DiO/DiD staining
  - Imaging
  - Attraction assay and optogenetics
  - Molecular cloning
  - Extracting connectivity data
  - Simulating membrane potential of neurons
  - Exploring different polarity combinations
  - Manipulation of synaptic strength values
  - Assessing the validity of each parameter set
  - Assessing the simulated response of the interneurons
  - Perturbations to the circuit's connectivity
- **QUANTIFICATION AND STATISTICAL ANALYSIS**

AUTHOR CONTRIBUTIONS

V.P. and Y.S. conducted the experiments. A.H.C., R.A.B., J.R.H., M.L.E., R.M.M., and N.J.R. contributed to behavioral experiments ("head-drop assays"). G.G. carried out all simulations and modeling experiments. D.S.P., D.M.F., E.S., and M.O.-S. supervised and designed experiments. V.P., Y.S., G.G., E.S., and M.O.-S. wrote the paper.

DECLARATION OF INTERESTS

The authors declare no competing interests.

INCLUSION AND DIVERSITY

We worked to ensure sex balance in the selection of nonhuman subjects. One or more of the authors of this paper self-identifies as a member of the LGBTQ+ community.

REFERENCES

1. Hashikawa, K., Hashikawa, Y., Lischinsky, J., and Lin, D. (2018). The neural mechanisms of sexually dimorphic aggressive behaviors. Trends Genet *34*, 755–776.

2. McKinsey, G., Ahmed, O.M., and Shah, N.M. (2018). Neural control of sexually dimorphic social behaviors. Curr. Opin. Physiol. *6*, 89–95.

3. Kimura, K., Hachiya, T., Koganezawa, M., Tazawa, T., and Yamamoto, D. (2008). Fruitless and doublesex coordinate to generate male-specific neurons that can initiate courtship. Neuron *59*, 759–769.

4. White, J.G., Southgate, E., Thomson, J.N., and Brenner, S. (1986). The structure of the nervous system of *Caenorhabditis elegans*. Philos. Trans. R. Soc. Lond. B Biol. Sci. *314*, 1–340.

5. Keddy-Hector, A.C., Wilczynski, W., and Ryan, M.J. (1992). Call patterns and basilar papilla tuning in cricket frogs. II. Intrapopulation variation and allometry. Brain Behav. Evol. *39*, 238–246.

6. McClelland, B.E., Wilczynski, W., and Rand, A.S. (1997). Sexual dimorphism and species differences in the neurophysiology and morphology of the acoustic communication system of two Neotropical hylids. J. Comp. Physiol. A *180*, 451–462.

7. Narins, P.M., and Capranica, R.R. (1976). Sexual differences in the auditory system of the tree frog Eleutherodactylus coqui. Science *192*, 378–380.

8. Shen, J.-X., Xu, Z.-M., Yu, Z.-L., Wang, S., Zheng, D.-Z., and Fan, S.-C. (2011). Ultrasonic frogs show extraordinary sex differences in auditory frequency sensitivity. Nat. Commun. *2*, 342.

9. Wilczynski, W., Zakon, H.H., and Brenowitz, E.A. (1984). Acoustic communication in spring peepers. J. Comp. Physiol. *155*, 577–584.

10. Wan, X., Zhou, Y., Chan, C.M., Yang, H., Yeung, C., and Chow, K.L. (2019). SRD-1 in AWA neurons is the receptor for female volatile sex pheromones in *C. elegans* males. EMBO Rep *20*, 715.

11. Ryan, D.A., Miller, R.M., Lee, K., Neal, S.J., Fagan, K.A., SenGupta, P., and Portman, D.S. (2014). Sex, age, and hunger regulate behavioral prioritization through dynamic modulation of chemoreceptor expression. Curr. Biol. *24*, 2509–2517.

12. He, J., Ma, L., Kim, S., Nakai, J., and Yu, C.R. (2008). Encoding gender and individual information in the mouse vomeronasal organ. Science *320*, 535–538.

13. Holy, T.E., Dulac, C., and Meister, M. (2000). Responses of vomeronasal neurons to natural stimuli. Science *289*, 1569–1572.

14. Cook, S.J., Jarrell, T.A., Brittin, C.A., Wang, Y., Bloniarz, A.E., Yakovlev, M.A., Nguyen, K.C.Q., Tang, L.T.-H., Bayer, E.A., Duerr, J.S., et al. (2019). Whole-animal connectomes of both *Caenorhabditis elegans* sexes. Nature *571*, 63–71.

15. Raisman, G., and Field, P.M. (1973). Sexual dimorphism in the neuropil of the preoptic area of the rat and its dependence on neonatal androgen. Brain Res *54*, 1–29.

16. Raisman, G., and Field, P.M. (1971). Sexual dimorphism in the preoptic area of the rat. Science *173*, 731–733.

17. Bayless, D.W., and Shah, N.M. (2016). Genetic dissection of neural circuits underlying sexually dimorphic social behaviours. Philos. Trans. R. Soc. Lond. B Biol. Sci. *371*, 20150109.

18. Cooke, B.M., and Woolley, C.S. (2005). Sexually dimorphic synaptic organization of the medial amygdala. J. Neurosci. *25*, 10759–10767.

19. Li, Y., and Dulac, C. (2018). Neural coding of sex-specific social information in the mouse brain. Curr. Opin. Neurobiol. *53*, 120–130.

20. Tikhonov, M., and Bialek, W. (2016). Complexity of generic biochemical circuits: topology versus strength of interactions. Phys. Biol. *13*, 066012.

21. Jang, H., Kim, K., Neal, S.J., Macosko, E., Kim, D., Butcher, R.A., Zeiger, D.M., Bargmann, C.I., and SenGupta, P. (2012). Neuromodulatory state and sex specify alternative behaviors through antagonistic synaptic pathways in *C. elegans*. Neuron *75*, 585–592.

22. Jarrell, T.A., Wang, Y., Bloniarz, A.E., Brittin, C.A., Xu, M., Thomson, J.N., Albertson, D.G., Hall, D.H., and Emmons, S.W. (2012). The connectome of a decision-making neural network. Science *337*, 437–444.

23. Stephens, G.J., Johnson-Kerner, B., Bialek, W., and Ryu, W.S. (2008). Dimensionality and dynamics in the behavior of *C. elegans*. PLoS Comput. Biol. *4*, e1000028.

24. Cohen, N., and Denham, J.E. (2019). Whole animal modeling: piecing together nematode locomotion. Curr. Opin. Syst. Biol. *13*, 150–160.

25. Brittin, C.A., Cook, S.J., Hall, D.H., Emmons, S.W., and Cohen, N. (2021). A multi-scale brain map derived from whole-brain volumetric reconstructions. Nature *591*, 105–110.

26. Bryden, J., and Cohen, N. (2008). Neural control of *Caenorhabditis elegans* forward locomotion: the role of sensory feedback. Biol. Cybern. *98*, 339–351.

27. McCarthy, M.M. (2021). SexX matters when it comes to pain. Neuron *109*, 1253–1254.

28. Mogil, J.S. (2020). Qualitative sex differences in pain processing: emerging evidence of a biased literature. Nat. Rev. Neurosci. *21*, 353–365.

29. Mogil, J.S. (2012). Sex differences in pain and pain inhibition: multiple explanations of a controversial phenomenon. Nat. Rev. Neurosci. *13*, 859–866.

30. Sorge, R.E., and Strath, L.J. (2018). Sex differences in pain responses. Curr. Opin. Physiol. *6*, 75–81.

31. Wiesenfeld-Hallin, Z. (2005). Sex differences in pain perception. Gend. Med. *2*, 137–145.

32. Sorge, R.E., Mapplebeck, J.C.S., Rosen, S., Beggs, S., Taves, S., Alexander, J.K., Martin, L.J., Austin, J.-S., Sotocinal, S.G., Chen, D., et al. (2015). Different immune cells mediate mechanical pain hypersensitivity in male and female mice. Nat. Neurosci. *18*, 1081–1083.

33. Yu, W., Pati, D., Pina, M.M., Schmidt, K.T., Boyt, K.M., Hunker, A.C., Zweifel, L.S., McElligott, Z.A., and Kash, T.L. (2021). Periaqueductal gray/dorsal raphe dopamine neurons contribute to sex differences in pain-related behaviors. Neuron *109*, 1365–1380.e5.

34. Bargmann, C.I., Thomas, J.H., and Horvitz, H.R. (1990). Chemosensory cell function in the behavior and development of *Caenorhabditis elegans*. Cold Spring Harb. Symp. Quant. Biol. *55*, 529–538.

35. Braendle, C., and Félix, M.-A. (2006). Sex determination: ways to evolve a hermaphrodite. Curr. Biol. *16*, R468–R471.

36. Thomas, C.G., Woodruff, G.C., and Haag, E.S. (2012). Causes and consequences of the evolution of reproductive mode in *Caenorhabditis nematodes*. Trends Genet *28*, 213–220.

37. Guo, Z.V., Hart, A.C., and Ramanathan, S. (2009). Optical interrogation of neural circuits in *Caenorhabditis elegans*. Nat. Methods *6*, 891–896.

38. Lindsay, T.H., Thiele, T.R., and Lockery, S.R. (2011). Optogenetic analysis of synaptic transmission in the central nervous system of the nematode *Caenorhabditis elegans*. Nat. Commun. *2*, 306.

39. Gjorgjieva, J., Biron, D., and Haspel, G. (2014). Neurobiology of *Caenorhabditis elegans* locomotion: where do we stand? BioScience *64*, 476–486.

40. Kawano, T., Po, M.D., Gao, S., Leung, G., Ryu, W.S., and Zhen, M. (2011). An imbalancing act: gap junctions reduce the backward motor circuit activity to bias *C. elegans* for forward locomotion. Neuron *72*, 572–586.

41. Patil, S., Zhou, K., and Parker, A.C. (2015). Neural circuits for touch-induced locomotion in *Caenorhabditis elegans*. In 2015 International Joint Conference on Neural Networks (IJCNN), pp. 1–8.

42. Zhen, M., and Samuel, A.D. (2015). C. elegans locomotion: small circuits, complex functions. Curr. Opin. Neurobiol. *33*, 117–126.

43. Miesenböck, G., De Angelis, D.A.D., and Rothman, J.E. (1998). Visualizing secretion and synaptic transmission with pH-sensitive green fluorescent proteins. Nature *394*, 192–195.

44. Bono, M. de, and Maricq, A.V. (2005). Neuronal substrates of complex behaviors in *C. elegans*. Annu. Rev. Neurosci. *28*, 451–501.

45. Culotti, J.G., and Russell, R.L. (1978). Osmotic avoidance defective mutants of the nematode *Caenorhabditis elegans*. Genetics *90*, 243–256.

46. Ferkey, D.M., SenGupta, P., and L'Etoile, N.D. (2021). Chemosensory signal transduction in *Caenorhabditis elegans*. Genetics *217*, iyab004.

47. Kaplan, J.M., and Horvitz, H.R. (1993). A dual mechanosensory and chemosensory neuron in *Caenorhabditis elegans*. Proc. Natl. Acad. Sci. USA *90*, 2227–2231.

48. Troemel, E.R., Chou, J.H., Dwyer, N.D., Colbert, H.A., and Bargmann, C.I. (1995). Divergent seven transmembrane receptors are candidate chemosensory receptors in *C. elegans*. Cell *83*, 207–218.

49. Serrano-Saiz, E., Oren-Suissa, M., Bayer, E.A., and Hobert, O. (2017). Sexually dimorphic differentiation of a *C. elegans* Hub neuron is cell autonomously controlled by a conserved transcription factor. Curr. Biol. *27*, 199–209.

50. Ventimiglia, D., and Bargmann, C.I. (2017). Diverse modes of synaptic signaling, regulation, and plasticity distinguish two classes of *C. elegans* glutamatergic neurons. eLife *6*, e31234.

51. Prinz, A.A., Bucher, D., and Marder, E. (2004). Similar network activity from disparate circuit parameters. Nat. Neurosci. *7*, 1345–1352.

52. Goodman, M.B., Hall, D.H., Avery, L., and Lockery, S.R. (1998). Active currents regulate sensitivity and dynamic range in *C. elegans* neurons. Neuron *20*, 763–772.

53. Palyanov, A., Khayrulin, S., Larson, S.D., and Dibert, A. (2011-2012). Towards a virtual *C. elegans*: a framework for simulation and visualization of the neuromuscular system in a 3D physical environment. Silico Biol *11*, 137–147.

54. Rakowski, F., and Karbowski, J. (2017). Optimal synaptic signaling connectome for locomotory behavior in *Caenorhabditis elegans*: design minimizing energy cost. PLoS Comput. Biol. *13*, e1005834.

55. Rakowski, F., Srinivasan, J., Sternberg, P.W., and Karbowski, J. (2013). Synaptic polarity of the interneuron circuit controlling *C. elegans* locomotion. Front. Comput. Neurosci. *7*, 128.

56. Roehrig, C.J. (1998). Computational model of a behaviour in *C. elegans* and a resulting framework for modularizing dynamical neuronal structures. PhD thesis (University of British Columbia).

57. Varshney, L.R., Chen, B.L., Paniagua, E., Hall, D.H., and Chklovskii, D.B. (2011). Structural properties of the *Caenorhabditis elegans* neuronal network. PLoS Comput. Biol. *7*, e1001066.

58. Wicks, S.R., Roehrig, C.J., and Rankin, C.H. (1996). A dynamic network simulation of the nematode tap withdrawal circuit: predictions concerning synaptic function using behavioral criteria. J. Neurosci. *16*, 4017–4031.

59. Fenyves, B.G., Szilágyi, G.S., Vassy, Z., Sőti, C., and Csermely, P. (2020). Synaptic polarity and sign-balance prediction using gene expression data in the *Caenorhabditis elegans* chemical synapse neuronal connectome network. PLoS Comput. Biol. *16*, e1007974.

60. Putrenko, I., Zakikhani, M., and Dent, J.A. (2005). A family of acetylcholine-gated chloride channel subunits in *Caenorhabditis elegans*. J. Biol. Chem. *280*, 6392–6398.

61. Chalasani, S.H., Chronis, N., Tsunozaki, M., Gray, J.M., Ramot, D., Goodman, M.B., and Bargmann, C.I. (2007). Dissecting a circuit for olfactory behaviour in *Caenorhabditis elegans*. Nature *450*, 63–70.

62. Taylor, S.R., Santpere, G., Weinreb, A., Barrett, A., Reilly, M.B., Xu, C., Varol, E., Oikonomou, P., Glenwinkel, L., McWhirter, R., et al. (2021). Molecular topography of an entire nervous system. Cell *184*, 4329–4347.e23.

63. Desbois, M., Cook, S.J., Emmons, S.W., and Bülow, H.E. (2015). Directional trans-synaptic labeling of specific neuronal connections in live animals. Genetics *200*, 697–705.

64. Mehra, A., Gaudet, J., Heck, L., Kuwabara, P.E., and Spence, A.M. (1999). Negative regulation of male development in *Caenorhabditis elegans* by a protein-protein interaction between TRA-2A and FEM-3. Genes Dev *13*, 1453–1463.

65. Mowrey, W.R., Bennett, J.R., and Portman, D.S. (2014). Distributed effects of biological sex define sex-typical motor behavior in *Caenorhabditis elegans*. J. Neurosci. *34*, 1579–1591.

66. Oren-Suissa, M., Bayer, E.A., and Hobert, O. (2016). Sex-specific pruning of neuronal synapses in *Caenorhabditis elegans*. Nature *533*, 206–211.

67. Rabinowitch, I., Chatzigeorgiou, M., Zhao, B., Treinin, M., and Schafer, W.R. (2014). Rewiring neural circuits by the insertion of ectopic electrical synapses in transgenic *C. elegans*. Nat. Commun. *5*, 4442.

68. Fan, Y., Yue, X., Xue, F., Cui, J., Brauth, S.E., Tang, Y., and Fang, G. (2018). Auditory perception exhibits sexual dimorphism and left telencephalic dominance in *Xenopus laevis*. Biol. Open *7*, bio035956.

69. Chiu, H., Hoopfer, E.D., Coughlan, M.L., Pavlou, H.J., Goodwin, S.F., and Anderson, D.J. (2021). A circuit logic for sexually shared and dimorphic aggressive behaviors in Drosophila. Cell *184*, 507–520.e16.

70. Hoke, K.L., Ryan, M.J., and Wilczynski, W. (2010). Sexually dimorphic sensory gating drives behavioral differences in túngara frogs. J. Exp. Biol. *213*, 3463–3472.

71. Hindmarsh Sten, T.H., Li, R., Otopalik, A., and Ruta, V. (2021). Sexual arousal gates visual processing during Drosophila courtship. Nature *595*, 549–553.

72. Towlson, E.K., Vértes, P.E., Ahnert, S.E., Schafer, W.R., and Bullmore, E.T. (2013). The rich club of the *C. elegans* Neuronal connectome. J. Neurosci. *33*, 6380–6387.

73. Fagan, K.A., Luo, J., Lagoy, R.C., Schroeder, F.C., Albrecht, D.R., and Portman, D.S. (2018). A single-neuron chemosensory switch determines the valence of a sexually dimorphic sensory behavior. Curr. Biol. *28*, 902–914.e5.

74. Wu, B., Ma, L., Zhang, E., Du, J., Liu, S., Price, J., Li, S., and Zhao, Z. (2018). Sexual dimorphism of sleep regulated by juvenile hormone signaling in *Drosophila*. PLoS Genet *14*, e1007318.

75. Goaillard, J.-M., and Marder, E. (2021). Ion channel degeneracy, variability, and covariation in neuron and circuit resilience. Annu. Rev. Neurosci. *44*, 335–357.

76. Kfir, Y., Renan, I., Schneidman, E., and Segev, R. (2012). The natural variation of a neural code. PLoS One *7*, e33149.

77. Körholz, J.C., Zocher, S., Grzyb, A.N., Morisse, B., Poetzsch, A., Ehret, F., Schmied, C., and Kempermann, G. (2018). Selective increases in inter-individual variability in response to environmental enrichment in female mice. eLife *7*, e35690.

78. Schneidman, E., Brenner, N., Tishby, N., Steveninck, R.R.de R. van, and Bialek, W. (2000). Universality and individuality in a neural code. Adv. Neural Inf. Process Syst. *13*, 159–165.

79. Zajitschek, S.R., Zajitschek, F., Bonduriansky, R., Brooks, R.C., Cornwell, W., Falster, D.S., Lagisz, M., Mason, J., Senior, A.M., Noble, D.W., et al. (2020). Sexual dimorphism in trait variability and its eco-evolutionary and statistical implications. eLife *9*, e63170.

80. Witvliet, D., Mulcahy, B., Mitchell, J.K., Meirovitch, Y., Berger, D.R., Wu, Y., Liu, Y., Koh, W.X., Parvathala, R., Holmyard, D., et al. (2021). Connectomes across development reveal principles of brain maturation. Nature *596*, 257–261.

81. Hosken, D.J., and House, C.M. (2011). Sexual selection. Curr. Biol. *21*, R62–R65.

82. Mead, L.S., and Arnold, S.J. (2004). Quantitative genetic models of sexual selection. Trends Ecol. Evol. *19*, 264–271.

83. Ezcurra, M., Tanizawa, Y., Swoboda, P., and Schafer, W.R. (2011). Food sensitizes *C. elegans* avoidance behaviours through acute dopamine signalling. EMBO J *30*, 1110–1122.

84. Katz, M., Corson, F., Keil, W., Singhal, A., Bae, A., Lu, Y., Liang, Y., and Shaham, S. (2019). Glutamate spillover in *C. elegans* triggers repetitive behavior through presynaptic activation of MGL-2/mGluR5. Nat. Commun. *10*, 1882.

85. Schindelin, J., Arganda-Carreras, I., Frise, E., Kaynig, V., Longair, M., Pietzsch, T., Preibisch, S., Rueden, C., Saalfeld, S., Schmid, B., et al. (2012). Fiji: an open-source platform for biological-image analysis. Nat. Methods *9*, 676–682.

86. Hilliard, M.A., Bargmann, C.I., and Bazzicalupo, P. (2002). C. elegans responds to chemical repellents by integrating sensory inputs from the head and the tail. Curr. Biol. *12*, 730–734.

87. Hilliard, M.A., Bergamasco, C., Arbucci, S., Plasterk, R.H.A., and Bazzicalupo, P. (2004). Worms taste bitter: ASH neurons, QUI-1, GPA-3 and ODR-3 mediate quinine avoidance in *Caenorhabditis elegans*. EMBO J *23*, 1101–1111.

88. Chronis, N., Zimmer, M., and Bargmann, C.I. (2007). Microfluidics for in vivo imaging of neuronal and behavioral activity in *Caenorhabditis elegans*. Nat. Methods *4*, 727–731.

89. Pradhan, S., Quilez, S., Homer, K., and Hendricks, M. (2019). Environmental programming of adult foraging behavior in *C. elegans*. Curr. Biol. *29*, 2867–2879.e4.

90. Thévenaz, P., Ruttimann, U.E., and Unser, M. (1998). A pyramid approach to subpixel registration based on intensity. IEEE Trans. Image Process. *7*, 27–41.

91. Gerstner, W., Kistler, W.M., Naud, R., and Paninski, L. (2014). Neuronal Dynamics (Cambridge University Press).

92. Piggott, B.J., Liu, J., Feng, Z., Wescott, S.A., and Xu, X.Z.S. (2011). The neural circuits and synaptic mechanisms underlying motor initiation in *C. elegans*. Cell *147*, 922–933.

93. Wicks, S.R., and Rankin, C.H. (1997). Effects of tap withdrawal response habituation on other withdrawal behaviors: the localization of habituation in the nematode *Caenorhabditis elegans*. Behav. Neurosci. *111*, 342–353.

94. Shindou, T., Ochi-Shindou, M., Murayama, T., Saita, E., Momohara, Y., Wickens, J.R., and Maruyama, I.N. (2019). Active propagation of dendritic electrical signals in *C. elegans*. Sci. Rep. *9*, 3430.

STAR★METHODS

KEY RESOURCES TABLE

REAGENT or RESOURCE	SOURCE	IDENTIFIER
Bacterial and virus strains		
OP50	Caenorhabditis Genetics Center	N/A
Deposited data		
Original code	Mendeley Data	https://doi.org/10.17632/kn7c893m62.1
Experimental models: Organisms/strains		
Caenorhabditis remanei	Caenorhabditis Genetics Center	PB4641
Caenorhabditis afra	Caenorhabditis Genetics Center	JU1286
him-5(e1490) V	Caenorhabditis Genetics Center	CB4088
lite-1(ce314); ljIs114[gpa-13p::FLPase, sra-6p::FTF::ChR2::YFP]	Ezcurra et al.[83]	AQ2235
lite-1(ce314); ljIs114; him-5(e1490) V	This paper	MOS52
etyIs1[gpa-13p::FLPase, sra-6p::FTF::GCaMP6s]; him-5(e1490) V 6X back-crossed	This paper	MOS88
otIs518[eat-4(fosmid)::SL2::mCherry::H2B, pha-1(+)]; him-5(e1490) V	Caenorhabditis Genetics Center	OH13645
kyIs673[sra-6p::eat-4::pHluorin, unc-122p::dsRed] UV integrated, backcrossed to N2 8x	Ventimiglia and Bargmann[50]	CX16921
kyEx4787 [rig-3p::iGluSnFR, unc-122p::dsRed]; kyEx4786 [rig-3p::RCaMP1e, unc-122p::GFP]	Katz et al.[84]	OS10227
kyIs673; kyEx4786; him-5(e1490) V	This paper	MOS198
etyEx35[flp-18p::GCaMP6s, ttx-3p::mCherry]; him-5(e1490) V	This paper	MOS134
etyEx70[pMO34(flp-18p::tra-2(IC)), unc-122p::gfp]; lite-1(ce314); ljIs114; him-5(e1490) V	This paper	MOS279
etyEx71[pMO30 (flp-18p::fem-3::SL2::2XNLS::tagRFP), unc-122p::gfp]; lite-1(ce314); ljIs114; him-5(e1490) V	This paper	MOS280
him-5(e1490)V; fsEx357[osm-5p::TRA-2ic::mCherry]	Fagan et al.[73]	UR754
fsEx357; lite-1(ce314); ljIs114; him-5(e1490) V	This paper	MOS369
him-5(e1490)V; fsIs22[osm-5p::fem-3::mCherry, unc-122p::GFP] (LG unknown)	This paper	UR1094
fsIs22; lite-1(ce314); ljIs114; him-5(e1490) V	This paper	MOS370
etyEx106[sra-6p::Cx36::YFP, flp-18p::Cx36::mCherry; unc-122p::GFP]; him-5(e1490) V	This paper	MOS374
N2: Ancestral from CGC	Caenorhabditis Genetics Center	WormBase ID: WBStrain00000003
etyEx22[ocr-2::GFP fosmid, ttx-3p::mCherry]; him-5(e1490) V	This paper	MOS100
nuIs11[osm-10::GFP, lin-15(+)]	Caenorhabditis Genetics Center	HA3
nuIs11; him-5(e1490) V	This paper	MOS69
etyEx86[qui-1::GFP fosmid, ttx-3p::mCherry]; him-5(e1490) V	This paper	MOS334
etyEx109[gpa-3::GFP fosmid, ttx-3p::mCherry]; him-5(e1490) V	This paper	MOS380
etyEx42[osm-9::GFP fosmid, ttx-3p::mCherry]; him-5(e1490) V	This paper	MOS192
etyEx121[sra-6p::BirA::nrx-1, pMO26 (flp-18p::AP::NLG-1), unc-122::streptavidin::2xsfGFP, MVC11 (flp-18p::mcherry), pRF4(rol-6)]; him-5(e1490)	This paper	MOS435
etyEx71; etyEx121; him-5(e1490)	This paper	MOS441
fsIs22; etyEx121; him-5(e1490)	This paper	MOS464
fsEx357; etyEx121; him-5(e1490)	This paper	MOS469
etyEx70; etyEx121	This paper	MOS474
unc-31(e928) IV	Caenorhabditis Genetics Center	DA509

(Continued on next page)

Continued

REAGENT or RESOURCE	SOURCE	IDENTIFIER
Oligonucleotides		
CCCAGCTTTCTTGTACAAAGTGGGAATGGTTGATTCAAGTAGAAGA	ASH-specific GCaMP6s	GCaMP3_F1
CACCATGGTGGCGGCCGCGGGTTTAGCCGTCATCATCTGAACG	ASH-specific GCaMP6s	GCaMP3_R1
CGTTCAGATGATGACGGCTAAACCCGCGGCCGCCACCATGGTG	ASH-specific GCaMP6s	sra-6bb_F1
TCTTCTACTTGAATCAACCATTCCCACTTTGTACAAGAAAGC	ASH-specific GCaMP6s	sra-6bb_R1
TAAAGAATTCCAACTGAGCGC	Masculinization and feminization of ASH	pTNZ109 F3u
TCCCACTTTGTACAAGAAAGCTG	Masculinization and feminization of ASH	pTNZ109 R3u
CAGCTTTCTTGTACAAAGTGGGAatggaattctcaatcaaacgatc	Masculinization and feminization of ASH	tra-2IC_SL2tagRFP_F1
GCGCTCAGTTGGAATTCTTTAtcagttggaattcgaagcttg	Masculinization and feminization of ASH	tra-2IC_SL2tagRFP_R1
CAGCTTTCTTGTACAAAGTGGGAatggaggtggatccgggttca	Masculinization and feminization of ASH	fem-3_SL2tagRFP_F1
AACTTTGTATAGAAAAGTTGAAATCTGTCACATACTGCTCGAATCG	AVA-specific Cx36 construct	MVC12_F
GCTTTTTTGTACAAACTTGTTTCGGGGGTAGATTTCAAATAGATTGG	AVA-specific Cx36 construct	MVC12_R
ATTTGAAATCTACCCCCGAAACAAGTTTGTACAAAAAAGCAG	AVA-specific Cx36 construct	pIR204_Fwd
GAGCAGTATGTGACAGATTTCAACTTTTCTATACAAAGTTGATAGC	AVA-specific Cx36 construct	pIR204_Rev
ttattatttcagattttgccGGATCCCCGGGATTGGCCAA	ASH-specific iBlinc construct	pMO22_Fwd
cgatttattatatctaaaagATTTCATTTCCAAGTTGTTAGCGTATCC	ASH-specific iBlinc construct	pMO22_Rev
CTAACAACTTGGAAATGAAATcttttagatataataaatcgaaattgaaatgt	ASH-specific iBlinc construct	Psra-6_Fwd
TTGGCCAATCCCGGGGATCCggcaaaatctgaaataataaatattaaattc	ASH-specific iBlinc construct	Psra-6_Rev
ggaggacccttggctagcATGGTTGATTCAAGTAGAAGAAAATG	AVA-specific GCaMP6s	Lada7F
ggcgctcagttggaattctTTAGCCGTCATCATCTGAAC	AVA-specific GCaMP6s	Lada7R
GCTAGCCAAGGGTCCTCCTGAA	AVA-specific GCaMP6s	GRASPbb _R1u
GAATTCCAACTGAGCGCCGGTCG	AVA-specific GCaMP6s	GRASPbb_F1u
Software and algorithms		
MATLAB	MathWorks	https://www.mathworks.com/products/matlab.html
FIJI	Schindelin et al.[85]	https://imagej.net/software/fiji/; https://doi.org/10.1038/nmeth.2019
BioRender	BioRender	https://biorender.com/
GraphPad Prism	GraphPad by Dotmatics	https://www.graphpad.com/scientific-software/prism/
Adobe Illustrator	Adobe	https://www.adobe.com
WormLab	MBF Bioscience	https://www.mbfbioscience.com/wormlab
ZEN	ZEISS	https://www.zeiss.com/microscopy/int/products/microscope-software/zen.html
Python – Spyder	Spyder IDE	https://www.spyder-ide.org/
Other		
Whole-animal connectomes of both Caenorhabditis elegans sexes	Cook et al.[14]	https://doi.org/10.1038/s41586-019-1352-7

RESOURCE AVAILABILITY

Lead contact
Further information and requests for resources and reagents should be directed to and will be fulfilled by the lead contact, Meital Oren-Suissa (meital.oren@weizmann.ac.il).

Materials availability
Unique strains generated in this study have been deposited at the Caenorhabditis Genetics Center. Requests for other strains and plasmids should be directed to the lead contact.

Data and code availability

- This paper analyzes existing, publicly available data. These accession numbers for the datasets are listed in the key resources table.
- All original code has been deposited at Mendeley Data [https://doi.org/10.17632/kn7c893m62.1] and is publicly available as of the date of publication. DOI is listed in the key resources table.
- Any additional information required to reanalyze the data reported in this paper is available from the lead contact upon request.

EXPERIMENTAL MODEL AND SUBJECT DETAILS

Wild-type strains were *C. elegans* variety Bristol, strain N2. Worms were maintained according to standard methods. Worms were grown at 20°C on nematode growth media (NGM) plates seeded with bacteria (*E. coli* OP50) as a food source. Sex and age of animals used for each experiment are indicated in the corresponding figures and legends. All transgenic strains used in this study are listed in the key resources table.

METHOD DETAILS

Repellent assay – tail-drop
Tail-drop avoidance assay was described previously.[66,86] All assays were done on 1-day adults. Briefly, worms were given ten minutes to habituate on a foodless NGM experiment plate, and then underwent 8-10 repellent stimulations with at least 2 minutes intervals between stimuli. A small drop of the repellent (glycerol in S basal, SDS or copper (CuSO4) in M13 buffer (30 mM Tris-HCl (pH 7.0), 100 mM NaCl, 10 mM KCl) was placed on the agar near the tail of a forward-moving animal, using a 10 μl glass-calibrated pipette (VWR International), pulled by hand on a flame to create two needles with reduced diameter. The pipette was mounted in a holder with a rubber tube, operated by mouth. A day before the experiment, unseeded NGM plates were taken out of storage at 4°C, dried for 2 h at 37°C, and then left on the bench. Scoring for each trial was binary (1 for reversal, 0 for no reversal) in a 4 s window. The avoidance index represents an average of the fraction of reversal responses (scored as reversing or not reversing) in 10 trials of each single animal. For the tail-drop assay of L3 animals, worms were kept separately following the assay until their sex was identifiable.

Repellent assay – head-drop
The head-drop assay was performed for the repellents glycerol, SDS, copper and quinine, in M13 buffer following the protocol described by Hilliard et al.[86,87] In each experiment, ∼15 young adult worms were placed on a dry unseeded NGM plate and given ten minutes to habituate before each worm was subjected to one head-drop test. Namely, a small drop of stimulus was placed in front of a forward-moving worm, which was then scored according to its movement direction during a 4 sec window. The drop was placed with a fresh capillary pulled on a flame. Each assay plate received a score according to the calculation: (Number of worms reversed) · 100/(Total number of worms tested on the plate). For each experiment, assays were repeated on at least 3 independent days.

Microfluidic chip fabrication and calcium imaging
Olfactory chips were fabricated according to Chronis et al.[88] with the help of the Nanofabrication Unit at the Weizmann Institute of Science. In short, a polydimethylsiloxane (PDMS) mixture was cast into premade 0.5-cm-high chip molds and allowed to solidify at 65°C for 3 h. Individual chips were cut by hand with a scalpel and then punctured to create fluidic inlets using a PDMS biopsy punch (Elveflow) 0.5 mm in diameter. The chips were attached to glass coverslips by exposing them to plasma for 30 s, then manually attaching them together and drying them on a hot plate for 1 h at 65°C. The tunnel height was 28 μM and the width at the worm's nose space was 24 μM.

The microfluidic chip was operated using two pumps that control the flow of buffer and stimulus into the microfluidic chip. The solutions were pushed through PVC tubes and stainless-steel connectors into the tunnels of the chip, and with a manual switch, we determined the arrival of the stimulus to the worm. Tubes were replaced between experiments and connectors cleaned with

ethanol. The pumping rate during experiments was ~0.005 ml/min. Loading the worm into the chip was done by placing the worm in a drop of S basal buffer, sucking the drop with a 1 ml syringe and inserting it into the relevant inlet of the chip. After proper worm positioning, 2 minutes were given for habituation prior to imaging with the lasers on. To prevent movement, 10 mM Levamisole was added to all solutions (except for the S basal solution used to load the worm). To visualize proper delivery of the stimulus to the worm, 50 μM rhodamine B was added only to the stimulus. If the worm moved or the flow was incorrect, the file was discarded and a second trial was performed with the same worm. No more than two trials were done with the same worm. Imaging was done with a Zeiss LSM 880 confocal microscope using a 40x magnification water objective. Imaging rate was 6.667 Hz, total imaging duration was 2 min, and stimulus duration was 20 sec. Stimulus was given at 20 to 40 sec from imaging initiation. For analysis, the GCaMP6s fluorescence intensity was measured using FIJI. All files were exported as tiff files, ROIs (regions of interest) of the somas were drawn manually to best represent the signal, and their mean gray values were exported. Downstream data processing was performed using MATLAB. For each worm, the baseline fluorescent level (F_0) was calculated by averaging the mean gray values of 100 frames (15 sec) before stimulus delivery. Then, for each frame, the ΔF was calculated by subtracting F_0 from the value of that time point, and the result was divided by F_0, to normalize differences in fluorescence baseline levels between individuals ($\Delta F/F_0$).

All statistical comparisons were done on the normalized data. For peak response comparisons, the maximal values of each worm from 20 to 60 sec of imaging were used. Response duration comparisons were done as in Pradhan et al.[89] In short, first, the response range was calculated for each worm (subtraction of the minimum value from the maximum value obtained in the time window of 20 to 60 sec of imaging). Then, the number of frames with above-threshold values were quantified for each worm (if $value_i \geq$ minimum $value_i +$ threshold $\cdot$ $range_i$), using a 5% threshold, and converted into percentages.

pHluorin imaging

1-day adult worms expressing sra-6::eat-4::pHluorin[50] were imaged in a microfluidic chip and a 40X magnification water objective of a confocal microscope, similarly to the calcium imaging procedure. Each animal was imaged with a z-stack of 28 slices, 14.78 μm thick. The duration of imaging was 210 sec or 35 frames, at an imaging rate of 0.1666 Hz, and the 0.5 M glycerol stimuli were given at 36-60 sec / 6-10 frame, 96-120 sec / 16-20 frame and 156-180 sec / 26-30 frame. The analysis was partially automated; all images were first processed to delete z-slices that did not contain any relevant signal, and then, all the remaining z-slices were summed and cropped in FIJI to retain only the axon of ASHL/ASHR. To resolve any movements of the worms, the movies were registered with the StackReg plugin[90] using a rigid body transformation. The ROIs were then drawn manually, and mean gray values were extracted. The $\Delta F/F_0$ normalization was performed with MATLAB, and the baseline fluorescent level (F_0) was calculated for each stimulus separately using the four frames before each stimulus. For the comparison of peak responses between the sexes, using the normalized data, the maximum value during each stimulus was found, and from that value was subtracted the maximum value during baseline (the baseline before that specific stimulus). Then, a median was calculated over the three technical repeats for each worm, and that value was used for the statistical comparison.

Optogenetics

We used worms that only express ChR2 in ASH neurons, using the intersectional approach (*gpa-13p::FLPase, sra-6p::FTF::ChR2::YFP*), and mutated in the *lite-1* gene, to ensure the measured behavioral responses are not due to the activity of the endogenous blue-light receptors, but due to ChR2 activity. Worms at the L4 developmental stage were selected a day before the experiment and separated into hermaphrodite and male control and experiment groups. They were transferred to newly seeded plates with 300 μl OP50 that was concentrated at 1:10. ATR was added only to the experiment groups' plates, to a final concentration of 100 μM ATR. As ATR is sensitive to light, all the plates were handled in the dark. Tracking and optogenetics were done on unseeded NGM plates. The day before the experiment, the plates were taken out of storage at 4°C, dried for 2 h in 37°C, and left on the bench overnight. On the experiment day, these plates were seeded with 30 μl OP50 (and ATR, only for the experiment group's plates). Experiments were performed at 24°C. The MBF bioscience WormLab tracking system was used to image and deliver the blue LED stimulations. To keep the worms in the camera's field of view, a plastic ring was placed on the agar and five worms were placed inside it. After 10 minutes of habituation, the worms were tracked for 69 sec with five 2-sec LED activations each, and 10 sec inter-stimulus interval (ISI). Recording started with 10 sec without LED. Analysis was performed manually. If the worm reversed during a 3 sec window (2 sec LED duration + one additional second), it received a score of one, otherwise a score of zero. The five results of each worm were averaged to a number between zero and one. If the worm touched the ring or was moving backwards while the LED turned on, the trial was not counted.

DiO/DiD staining

Worms were washed with M9 buffer and incubated for 1 h in 1 ml M9 and 5 μl DiO/DiD dye in ~25 rpm tilt. The worms were then transferred to a fresh plate and let to crawl on a bacterial lawn.

Imaging

Prior to imaging, worms were mounted on a 5 % agarose pad on a glass slide, on a drop of M9 containing 100 mM sodium azide, which was used as an anesthetic. A Zeiss LSM 880 confocal microscope was used with 63x magnification, and all imaging parameters were kept identical in each imaging experiment. The thickness of the z-plane was different for each worm, to capture all the fluorescence present in the head (~40 μm for hermaphrodites, ~31 μm for males).

For the EAT-4/VGLUT expression measurement, ASH was identified based on its morphological position relative to all the stained DiO neurons, and the single z-plane with the strongest signal was exported for each worm to measure fluorescence intensity using FIJI. ROIs were manually drawn.

For the ASHp::ChR2::YFP expression measurement, maximum intensity projections were produced and the tif files were exported to FIJI. The images were converted to 16-bit black and white, and a threshold was applied to remove background noise (threshold settings - minimum threshold of 14, dark background and over/under). Manual ROIs were drawn around the somas and gray mean values were extracted for statistical quantification.

For the quantification of signaling molecules and receptors expressed in ASH (Figure S3B), the red channel (DiD imaging) was used to identify which slices of the z-stack of the whole head contain ASH soma (about 11 slices). The rest of the slices were removed from the z-stack of the GFP reporter channel. The slices that now contain specifically ASH soma were converted to a maximum intensity projection image, on which an ROI was drawn manually around ASH soma, and without containing signals from other neurons. The mean gray value was extracted and used for statistical comparisons.

Attraction assay and optogenetics

All preparations for the attraction assay were identical to the preparations of the optogenetic experiments. 2 μl of 10 mM sodium azide were placed on a dried, unseeded NGM plate and allowed to dry for ∼5 minutes. Then, a plastic ring ∼5 mm in diameter was placed on the plate, and 15 *unc-31* hermaphrodites were placed in the area with the absorbed sodium azide. A single male was placed each time inside the ring on the side opposite to the location of the hermaphrodites, and immediately a recording started with blue LED activations (1.47 mW/mm^2 LED intensity, 2 sec duration, 10 sec ISI). When the male touched a hermaphrodite, the recording and optogenetic activations were terminated, the male was removed from the plate, and a new male was added for the next trial. The time it took the male to reach the hermaphrodite served as its score for the statistical comparison. If the male did not reach a hermaphrodite within 20 minutes, the trial was terminated and discarded from the statistics.

Molecular cloning

The intersectional approach was employed to achieve ASH-specific expression.[83] pTNZ141 (*gpa-13p::FLPase*) was injected with a version of pTNZ109 (*sra-6p::FTF::ChR2::YFP*) in which the ChR2::YFP cassette was replaced with the transgene of interest. For calcium imaging of ASH, ChR2::YFP was replaced with GCaMP6s, amplified from p45.641 (*mec-4p-nls-RSET-GCaMP3(CEopt)-SL2-nls-TagRFP-unc-54utr*, a kind gift from Doug Kim).

Pan-sensory masculinization and feminization were achieved in a set of ciliated neurons by expressing *tra-2[intracellular]*[73] or *fem-3* under the *osm-5p*.

For calcium imaging of AVA, the GCaMP6s fragment was amplified from p45.641 and inserted into a backbone containing the *flp-18p* promoter by Gibson assembly. See key resources table for primers.

To create the iBlinc synaptic labeling between ASH and AVA, a *sra-6p* promoter fragment (for the ASH side) was linked to the birA::nrx-1 backbone by Gibson assembly. The resulting plasmid was injected with the plasmid pMO26 (*flp-18p::AP::NLG-1*) for the AVA side.

To generate an artificial gap junction between ASH and AVA, a *flp-18p* promoter fragment (for the AVA side) was inserted instead of the *gpa-11p* promoter in plasmid pIR204 (*gpa-11p::Cx36::mCherry*) by Gibson assembly. The resulting plasmid was injected with the plasmid pIR111 encoding for ASH-specific Cx36, *sra-6p::Cx36::YFP* (pIR111 and pIR204 were a kind gift from Ithai Rabinowitch).

Extracting connectivity data

Connectivity data was taken from Cook et al.[14] The strength of connectivity between each pair of neurons was described as the total number of electron-microscopy sections containing that connection. For the simulation, we used the average of the corresponding synaptic connections of the neurons in the left side and right side of the worm (ASH, AVA, AVB, AVD, PVC neurons) from Cook et al.,[14] and each neuronal group (A and B neurons), and they were treated as a single cell.[55] Connections within a neuronal class were ignored. Chemical synapses between neural groups or pairs were simulated if they appeared in more than 10 serial sections. We note that these criteria neglect possible asymmetry between the right and left side of the worm, as well as differences between the ventral and dorsal side, and that lumping together all neurons of the same class, does neglect possible structure within the class.

Simulating membrane potential of neurons

The membrane potential of the neurons in the circuit was calculated according to Varshney et al.[57] and Gerstner et al.:[91]

$$\frac{dV_i}{dt} = \frac{\sum_j \left(V_j^{gap} - V_i\right) \cdot \frac{g_{gap}}{g_m} \cdot S_{ij}^{gap} + \sum_j \theta \cdot \left(V_j^{chem} - V_i^{rest}\right) \cdot \frac{g_{chem}}{g_m} \cdot S_{ij}^{chem} - \left(V_i - V_i^{rest}\right) + RI}{\tau_m},$$

where V_i is the voltage of the postsynaptic neuron, V_j is that of its presynaptic partners, and the sums are over all neurons in the circuit. *rest* denotes the membrane potential at the resting state, *chem* and *gap* denote chemical synapses and gap junctions, respectively. g denotes conductance, and g_m is the membrane conductance of neuron i. S_{ij} is the strength of connection between

neuron i and neuron j. R is the input resistance of the neuron (R_{in}), I is the external current, and τ_m is the membrane time constant. θ is an indicator of the activity of chemical synapses:

$$\theta \begin{cases} 1 \ for \ \left(V_j^{chem} \ - \ V_j^{rest} \right) > 0 \\ 0 \ for \ \left(V_j^{chem} \ - \ V_j^{rest} \right) \leq 0 \end{cases},$$

such that chemical synapses are active only when the presynaptic cell is activated (i.e., above its resting potential). The neurons in this circuit are assumed to release neurotransmitters tonically and to not use action potentials.[57] We, therefore, simulated the effect of a chemical synapse as proportional to the strength of activation of the presynaptic cell (voltage above its rest value). We simulated the membrane potential of the neurons for 15 seconds, with time steps Δt = 0.2 ms. The sensory stimulus was presented as an external input current to the head sensory neuron ASH for 5 sec, starting from the 5th second of the simulation. To replicate the spontaneous forward movement of the worms, we assumed a basal activation of interneurons AVA, AVB, PVC – as these neurons' spontaneous activity correlated with the direction of the movement.[40,92,93] The basal inputs to the interneurons were "on" throughout the simulation.

As the values of different biophysical parameters of the neurons in this circuit are unknown, we used 7 different parameters for the simulations. For each parameter, we used 7 different values that were equally spaced on a logarithmic scale from a biologically reasonable range.[38,52–58] Specific membrane resistance (R_m) values were within 15 k$\Omega \cdot$cm^2 -1500 k$\Omega \cdot$cm^2. This range was chosen around the 150 k$\Omega \cdot$cm^2 value, used in multiple studies.[53,55,56] To maintain a relationship between Rm and Rin, we chose to fix the surface area of the neurons and set it to be 15$\cdot$10^{-6} cm^2 as was observed in Rakowski et al.,[55] Roehrig,[56] and Wicks et al.[58] R_{in} was calculated separately for each set of parameters, using the changing value of R_m and the fixed value of the surface area. This calculation resulted in values which match R_{in} values previously reported, ranging from ~2 GΩ,[40,94] to ~11 GΩ.[53,55,56,58] Specific capacitance values (Cm) were 0.1 $\frac{uF}{cm^2}$ -10 $\frac{uF}{cm^2}$.[52–54,56] We chose a range around the value of 1 $\frac{uF}{cm^2}$ which is a standard value for membrane capacitance.[56] Values of conductance of gap junctions and chemical synapses were 1 pS-1 nS.[55,58] Basal input values of the interneurons triggered a voltage change of 1 mV-75 mV. We chose the upper bound to be the strength of a strong sensory stimulus, and the minimal value as such that would only trigger a small change (1 mV). Overall, we explored 7^7=823,543 parameter combinations. The specific parameters of all the neurons in the circuit were assumed to be the same. To induce a voltage-change of a desired magnitude, we calculated the currents to the sensory neurons and to the interneurons, using the values of each parameter set.

Exploring different polarity combinations

In the circuits of both sexes there are 18 chemical synapses combined: 15 sex-shared, 2 hermaphrodite-specific, and 1 male-specific. For each parameter set we simulated all options of a single inhibitory synapse, on top of an all-excitatory state. This resulted in 823,543 · 19 = 15,647,317 combinations. In addition, for each parameter set we simulated all options of inhibitory and excitatory connections in the following connections: AVB-AVA, A-B, B-A, ASH-AVB (16 polarity options).

Manipulation of synaptic strength values

For each parameter and polarity set, the synaptic strength values were randomly and independently strengthened in 20%, weakened in 20%, or left unchanged.

Assessing the validity of each parameter set

All combinations of the parameter values and polarity options were evaluated to determine whether they would result in behavior that matched that of the experimentally observed one. To qualify, the parameter set had to meet the following behavioral conditions: First, the membrane potential of all the neurons had to remain lower than 100 mV throughout the simulation, and the time constant had to be lower than 500 ms. Second, the membrane potential of all the neurons had to move back toward the resting potential once the stimulus was over. Namely, the difference between the average membrane potential of each neuron at the last second of the simulation (4 seconds after the termination of the sensory stimulus) and the second before the sensory stimulus, had to be smaller than the difference between the termination time of the sensory stimulus, and the second before it began. Since in the absence of external stimuli worms typically move forward, we required the membrane potential of motor neuron B in the absence of a sensory stimulus to be higher than that of motor neuron A, which would result in a forward movement. Accordingly, we required backward movement in our simulation (A higher than B), after a strong sensory input. Those conditions were tested by comparing the average membrane potential of those cells in the second before the sensory stimulus began and at the last second the stimulus was given. The same conditions were applied for both the male's circuit and the hermaphrodite's circuit. Overlapping sets were defined as parameter sets that met the conditions for both sexes. On top of the behavioral conditions, we added additional physiological conditions, that were applied only for the hermaphrodites' circuitry: anticorrelated activity between the interneurons AVA and AVB (namely, AVB is higher before the stimulus begins, during the forward movement, and AVA is higher following the sensory stimulus during the backward movement). Moreover, we required an increase in activation of the neurons AVA and A following the sensory stimulus, alongside with a decrease in the activation of AVB and B. Appropriate sets, that were used in the rest of the model analyses, met all behavioral conditions for both sexes, and the physiological conditions for the hermaphrodites.

Assessing the simulated response of the interneurons

For the sets of parameters and polarity (ASH-AVB inhibitory) that met all conditions, we focused on stimuli that induced specific changes to the membrane potential of the sensory neurons (75mV, 45mV, 15mV, 1mV). For each set and stimulus value, we measured the resulting change in membrane potential in the interneurons AVA, AVB, AVD. The change was measured as the difference between the average membrane potential value at the last second of the sensory stimulus and the average membrane potential at the second before the stimulus began.

Perturbations to the circuit's connectivity

For each appropriate set, we simulated three kinds of perturbations: removing or adding a single dimorphic connection, removing or adding two dimorphic connections simultaneously, or replacing the connectivity of an individual neuron (here all connections of a specific cell were copied from the opposite sex - incoming and outgoing synapses and gap junctions); non-dimorphic connections were altered as well, and received the strength of the connection in the opposite sex. For each perturbation, we examined the response of the simulated circuits to multiple strengths of sensory stimuli.

QUANTIFICATION AND STATISTICAL ANALYSIS

Significance was computed using the GraphPad Prism software (version 9). Bar graphs are a box-and-whiskers type of graph, min to max showing all points. The vertical bars represent the median and "+" represents the mean. Hermaphrodite data is shown in orange, male in cyan. Statistical test parameters, outcomes and reporting on number of animals used in each experiment are indicated in figure legends.